Title

Seasonal wind stress direction influences source and properties of inflow to the Salish Sea and Columbia River estuary

Authors

Elizabeth Brasseale[1] (corresponding author) and Parker MacCready[2]

Affiliation

[1] University of Washington, School of Marine and Environmental Affairs, 3707 Brooklyn Ave NE, Seattle, WA 98195-5351, USA

[2] University of Washington, School of Oceanography, Box 355351, Seattle, WA 98195-5351, USA

Author Contact Information

eabrasse@uw.edu, pmacc@uw.edu

Key points

1. Inflow to the Salish Sea and Columbia River comes from north during upwelling-favorable winds and south during downwelling-favorable winds.
2. Inflow source is denser and relatively (but not absolutely) deeper during upwelling-favorable wind stress.
3. The Juan de Fuca canyon influences all inflow to the Salish Sea regardless of wind direction.

Abstract

Estuaries in the northern California current system (NCCS) experience seasonally reversing wind stress, which is expected to impact the origin and properties of shelf water which enters NCCS estuaries ('shelf inflow'). Wind stress has been shown to affect the source of shelf inflow by driving alongshelf currents. However, the effects of wind-driven Ekman dynamics and shelf currents from larger-scale forcing on shelf inflow have yet to be explored. Variations in shelf inflow to the Salish Sea and the Columbia River estuary, two large NCCS estuarine systems, were studied using a realistic hydrodynamic model. The paths and source of shelf water were identified using particles released on the shelf. Particles were released every two weeks of 2017 and tracked for sixty days. Shelf inflow was identified as particles that crossed the estuary mouths. Mean wind stress during each release was compared with initial horizontal and vertical positions and physical properties of shelf inflow particles. For both the Salish Sea and the Columbia River estuary, upwelling-favorable wind stress was correlated with a shelf inflow source north of the estuary mouth. Depth was not correlated with wind stress for either estuary, but relative depth (depth scaled by isobath) increased during upwelling-favorable winds for both. Properties of inflow changed from cold and fresh during upwelling to warm and salty during downwelling, reflecting seasonal changes in NCCS shelf waters. These results may be extended

to predict the source and properties of shelf inflow to estuaries in other regions with known wind or shelf current patterns.

Plain language summary

The seawater in estuaries brings in ocean-borne density, nutrients, and oxygen levels. To better predict estuarine conditions due to seasonal and longer scale ocean changes, we investigate where estuarine seawater originated in the ocean and why. Here we examine how seasonal wind direction impacts the location and properties of seawater in two Pacific northwest estuaries by generating flow pathways throughout the year 2017 using a 3D ocean forecast model. When wind was from the north (typical during Pacific northwest summer), estuarine seawater originated from the ocean to the north of the estuary mouth. During wintertime, wind from the south brought in seawater from south of the estuarine mouth. On average, seawater came from the same depth below the sea surface regardless of wind direction. However, under northerly winds, most seawater originated near the seafloor of the continental shelf, while under southerly winds, some seawater originated further offshore where the seafloor is much deeper. Since seawater near the seafloor tends to have lower oxygen, these flow pathways help to explain why seawater with low oxygen has been found entering Pacific northwest estuaries during summertime. These results can be extended to estuaries in other regions with known wind patterns.

Keywords

Estuary, shelf, inflow, particles, upwelling

1. Introduction

Estuaries mix buoyant water with coastal ocean water which originated somewhere on the continental shelf (hereafter "shelf inflow"). In idealized numerical models without atmospheric forcing, shelf inflow originates from the direction of coastal trapped wave propagation (Beardsley and Hart, 1978; Masse, 1990; Brasseale and MacCready, 2021). However, when wind stress forcing has been included, the source of shelf inflow was sourced from the upwind direction (Beardsley and Hart, 1978; Masse, 1990). An upwind shelf inflow source would be particularly consequential for estuaries in the northern California Current system (CCS) where wind direction switches between predominately upwelling-favorable in summer and downwelling-favorable in winter (Hickey and Banas, 2003).

Previous shelf inflow source investigations sought simple steady state numerical solutions to the momentum and continuity equations for a two-layer shelf, with a lower shelf inflow layer and an upper estuarine outflowing layer (Beardsley and Hart, 1978; Masse, 1990). However, since two-layer models do not resolve boundary layers, the effect of wind-driven Ekman layer transport on the shelf inflow source remains to be shown. Under upwelling-favorable wind stress, Ekman transport in the surface layer diverges at the coastline, creating upward flow through the bottom boundary layer. This is consistent with observations of dense shelf inflow to CCS estuaries during upwelling-favorable wind stress (Hickey et al., 2002). Intrusions of hypoxic shelf water to the Columbia River estuary have been observed in response to coastal upwelling (Roegner et al., 2011). Inflow to the Salish Sea, a large inland sea in the northern CCS shared by the United States and Canada, has been observed to originate in the Juan de Fuca canyon during upwelling-favorable winds (Alford and MacCready, 2014), and deep water believed to originate below the

shelf has been observed in the inland branches of the Salish Sea, including Puget Sound, during the upwelling-favorable wind season (Feely et al., 2010). Deep Pacific Ocean water has low aragonite saturation state and low pH, which may interfere with the growth of juvenile oyster and krill populations that reside in Puget Sound (McLaskey et al., 2016). Although deep water was observed to pass through the Juan de Fuca canyon during upwelling-favorable winds, it is still unknown, however, whether inflow to the Strait of Juan de Fuca originates in the Juan de Fuca canyon under downwelling-favorable winds. Observations presented in Cannon (1972) suggest that it does not, at least near the seaward end of the canyon at the shelf break. The effect of downwelling-favorable wind stress on estuarine inflow is less well-studied than upwelling.

Here, we investigate how upwelling- and downwelling-favorable wind stress impact the source of shelf inflow. This will be tested in two estuarine systems in the northern CCS, the Salish Sea and the Columbia River estuary. The Salish Sea and Columbia River estuary represent two different estuarine types: the Salish Sea is a glacially carved inland sea which functions as a fjord-like estuary, and the Columbia River estuary is a drowned river valley estuary. This study will focus on event scale (multi-day) forcing, as that is the time scale relevant for upwelling processes observed on the Oregon shelf (Austin and Barth, 2002). The effects of wind stress variations on shorter time scales (such as sea breeze) will be neglected. For each estuary, we will address the following questions:

1. Does inflow originate in the upwind direction?
2. Is upwelling-favorable wind stress associated with a deeper source of inflow?
3. Is the direction of wind stress correlated with different source water properties (density, temperature, and salinity)?

Addressing these questions will help explain seasonal variations in source waters to northern CCS estuaries and predict the source of shelf inflow to estuaries in other regions, including those with unidirectional wind stress (e.g., the southern CCS) or persistent coastal currents (e.g., the east coast of the United States).

2. Methods

2.1 Model set-up

Experiments were performed using the LiveOcean model (MacCready et al., 2021), which encompasses the Salish Sea and all coastal waters of Oregon, Washington, and Vancouver Island. The LiveOcean model was built using Regional Ocean Modeling System (ROMS), a three-dimensional Reynolds-averaged Navier-Stokes model that uses a terrain-following vertical coordinate (Shchepetkin and McWilliams, 2005). The horizontal resolution is 500 m in most of the Salish Sea and Washington coast, stretching up to 3 km at open boundaries. The model has 30 vertical levels, following the bathymetry and free surface. The model is configured with realistic forcing which includes 45 rivers, 8 tidal constituents, open ocean conditions from a global data-assimilative model, and high-resolution atmospheric forcing from a regional weather forecast model. The model hindcast has been extensively compared to observations (MacCready et al 2021).

2.2 Particle tracking scheme

Particle tracking experiments determined where inflow originated on the shelf. The shelf is seeded with particles which are passively advected by the ocean currents and mixed vertically by turbulence, modeled as a random walk following the technique developed by Visser (1997).

Particles were identified as estuarine inflow if, at any point after their release, they crossed a spatial line demarcating the estuarine channel entrance. The particle tracking algorithm forward-integrated a particle's position using the currents interpolated in time from saved hourly snapshots from the model. The forward integration scheme used is 4th-order Runge-Kutta with a 300-second time step to resolve tides, similar to that used in Banas et al. (2009), Giddings et al. (2014), Brasseale et al. (2019), Brasseale and MacCready (2021), and Xiong and MacCready (2023). A nearest-neighbor search algorithm was used for finding the velocities used to advect particles.

To examine inflow to the Strait of Juan de Fuca, approximately 260,000 particles were released at every 15 m of depth for 10,000 latitude-longitude pairs (100 evenly spaced positions between 47 and 49 N and 100 evenly spaced positions between -126 and -124 E; Figure 1a). The particles with release points on land or within the Strait of Juan de Fuca were masked out. To examine inflow to the Columbia River estuary, approximately 60,000 particles were released at every 30 m of depth for 1600 latitude-longitude pairs (40 evenly spaced positions between 44 and 48 N and 40 evenly spaced positions between -126 and -124 E; Figure 1b). For both estuaries, particles were released every two weeks throughout the year 2017 (26 total releases) and tracked for 60 days to sample the seasonal range of wind stresses experienced in the northern CCS.

Upwelling or downwelling in the ocean as a response to wind stress was estimated using a weighted average of the wind stress over the previous 8 days (hereafter "AB8d filter"), the time scale for upwelling fronts to reach dynamic equilibrium on the Oregon shelf (Austin and Barth, 2002). Analyses used the north-south component of wind stress extracted from the model at

longitude -125 and latitude 47.5, a location between the shelf and the slope approximately equidistant from the Strait of Juan de Fuca and the Columbia River estuary (Figure 2). Year 2017 was chosen for these experiments because the timing and duration of upwelling-favorable wind stress was typical for the region, i.e. consistent with upwelling-favorable wind conditions from interannual average from a nearby National Data Buoy Center mooring with wind data available from 2003 to 2020 (Figure 2).

3. Results

Wind stress was predominantly downwelling-favorable from January 1 to May 1, as typical for winter in the northern CCS. Wind stress was predominantly upwelling-favorable from May 1 to mid-October. From mid-October to the end of the year, wind stress returned to being predominantly downwelling-favorable. Mean AB8d-filtered downwelling-favorable wind stress for the study period was $\tau_y = 0.07$ Pa, more than twice the magnitude of the mean AB8d-filtered upwelling favorable wind stress of $\tau_y = -0.03$ Pa (Figure 2).

The particle releases experienced a mix of both upwelling- and downwelling-favorable wind stress. A release was categorized as representing upwelling- or downwelling-favorable wind stress using the sign of mean wind stress, $\overline{\tau_y}$, during the 60-day release. Of the twenty-six total releases for each estuary, eight releases represented upwelling-favorable conditions and fifteen releases represented downwelling-favorable conditions. The remaining three releases had $|\overline{\tau_y}| <$ 0.01 Pa and were therefore not considered representative of either upwelling- or downwelling-favorable conditions (Figure 3a).

The number of inflowing particles for a given release to the Strait of Juan de Fuca was an order of magnitude greater than the Columbia River estuary ($O(100)$ vs $O(10)$; Figure 3b vs c). There was no significant correlation between the number of inflowing particles and the strength or direction of wind stress.

3.1 Effect of wind stress on horizontal inflow source

In both experiments, the initial horizontal positions of inflowing particles were strongly correlated with the magnitude and direction of N-S wind stress (Figure 4a–b).

During upwelling-favorable wind stress, most inflowing particles to the Strait of Juan de Fuca were sourced from Vancouver Island shelf northwest of the Strait. Of all inflowing particles, 56% originated on the Vancouver Island shelf, compared with 6% from the Washington shelf and 0% from the Oregon shelf. The remaining 38% originated offshore of the shelf break (Figure 3b; Figure 5a). The strongest mean upwelling-favorable wind stress occurred for the 6/18/2017 release (Figure 5c–d). One case study particle began on the Vancouver Island shelf flowing southeast parallel to the coastline until it reached the Juan de Fuca canyon (thicker, darker line in Figure 5c–d). At the Juan de Fuca canyon, the particle trajectory bent 90° counterclockwise and travelled northeast. Once inside the Strait of Juan de Fuca, the trajectory turned 90° clockwise following Juan de Fuca canyon bathymetry. This case study particle was typical of most particles that originated on the Vancouver Island shelf during the 6/18/2017 release. All particles were steered by the Juan de Fuca canyon towards the Strait of Juan de Fuca, and none originated on the shelf south of the canyon. Some inflowing particle trajectories circulated in the Juan de Fuca eddy. A few particles originated below the shelf break and these reached the shelf through Juan de Fuca canyon or, in rare cases, directly across the shelf break after flowing northward.

196

197 During downwelling-favorable wind stress, most inflowing particles to the Strait of Juan de Fuca
198 originated off the shelf or on the shelf to the south of the Strait (Figure 3b; Figure 6a). Over half,
199 58%, of inflowing particles originated offshore of the shelf break. The Washington shelf was the
200 source of 33% of inflowing particles and 2% originated as far south as the Oregon shelf. Only
201 7% of inflowing particles during downwelling-favorable wind stress originated on the
202 Vancouver Island shelf. The 11/5/2017 release tracks were plotted as a representative
203 downwelling case for the Strait of Juan de Fuca, with one particle track highlighted (Figure 6c–
204 d). The highlighted particle begins on the Washington shelf and flows north, bending to the right
205 when it reaches the Juan de Fuca canyon. In this example release, most other inflowing particles
206 originated on the Washington shelf and followed a similar trajectory. Some particles originated
207 beyond the shelf break and travelled in a northward slope current parallel to the shelf current.
208

209 The Columbia River estuary results were consistent with the Strait of Juan de Fuca results,
210 although there were fewer inflowing particles overall. For inflowing particles released during
211 upwelling-favorable wind stress, 53% originated on the Washington shelf north of the Columbia
212 River estuary mouth, compared with 30% from the Oregon shelf to the south and 1% from the
213 Vancouver Island shelf. The remaining 16% originated offshore of the shelf break (Figure 3c;
214 Figure 7a). The 6/4/2017 release tracks were plotted as a representative upwelling release
215 because that release had the second strongest mean upwelling-favorable wind (Figure 7c–d). The
216 6/18/2017 release had the strongest mean upwelling-favorable wind, but it was not considered
217 representative because it resulted in the fewest inflowing particles. One typical particle track
218 from the representative release was highlighted in bold (Figure 7c–d). The highlighted particle

219 track began on the shelf and traveled southward, parallel to isobaths. It overshot the estuary
220 mouth before reversing and flowing in. The other inflowing particles from this release follow
221 similar southward shelf trajectories.
222
223 During downwelling-favorable wind stress, inflowing particles to the Columbia River estuary
224 originated mostly from south of the estuary mouth. The Oregon shelf was the source of 48% of
225 inflowing particles, compared with 17% from the Washington shelf and 0% from the Vancouver
226 Island shelf. The remaining 35% originated offshore of the shelf break. Thus, inflow from
227 offshore composed a larger proportion of inflowing particles during downwelling than
228 upwelling-favorable wind stress (Figure 3c; Figure 8a). The 10/22/2017 release had the strongest
229 downwelling-favorable wind and was plotted as a representative downwelling case, with one
230 typical particle track highlighted (Figure 8c–d). The highlighted particle began flowing
231 southward over the slope before moving eastward onto the shelf. Once on the shelf, it travelled
232 northward parallel to isobaths and entered the Columbia River estuary mouth. Other inflowing
233 particles that began offshore of the shelf break during the 10/22/2017 release followed similar
234 trajectories. Inflowing particles that began on the shelf travelled northward. A few overshot the
235 mouth before inflowing.
236
237 *3.2 Effect of wind stress on inflow source depth*
238 Vertical position was quantified using three metrics of initial inflowing particle position: vertical
239 position (meters from mean sea surface, up defined positive), relative vertical position (vertical
240 position divided by water column height, seafloor defined -1, sea surface defined 0), and the
241 isobath over which the particle originated (positive distance from sea floor to mean sea surface).

In neither estuary was the mean initial vertical position of inflowing particles correlated with wind stress direction or magnitude (Figure 4c–d). However, both estuaries had correlations between wind stress and mean relative vertical position and isobath of inflowing particles (Figure 4e–h), and both correlations were stronger for the Strait of Juan de Fuca (R^2=0.79 and R^2=0.62, respectively) than the Columbia River estuary (R^2=0.55 and R^2=0.29, respectively). The correlation between wind stress and isobath was consistent with the result that both the Strait of Juan de Fuca and the Columbia River estuary had more inflowing particles with initial positions over the slope during downwelling-favorable wind stress (compare Figure 5b with Figure 6b for Strait of Juan de Fuca; Figure 7b with Figure 8b for Columbia River estuary). Most slope-sourced particles originated above 200 m (middle slope water). For inflow to the Strait of Juan de Fuca, particles that originated below 200 m were mostly concentrated near the Juan de Fuca canyon.

3.3 Effect of wind stress on source water properties

We hypothesized that upwelling-favorable wind stress would result in a denser inflow source. However, density was weakly correlated with wind stress for mean inflow to the Strait of Juan de Fuca (Figure 4i) and not correlated for the Columbia River estuary (Figure 4j). The range of initial particle densities extended lower for the Columbia River estuary. The temperature-salinity composition of inflowing seawater varied for both estuaries with wind stress direction (Figure 9). Inflowing particles were colder and fresher during upwelling-favorable wind stress and warmer and saltier during downwelling-favorable wind stress. For the Strait of Juan de Fuca, releases during downwelling-favorable wind stress included inflowing particles with a range of fresher initial salinities around a fixed temperature (near 11° C in the representative 11/5/2017 release).

These fresher inflow particles represented the Columbia River estuary plume inflowing to the Strait of Juan de Fuca, a well-documented phenomenon that occurs during downwelling-favorable wind stress (Thomson et al., 2007; Giddings and MacCready, 2017). Columbia River estuary plume intrusions would lower the mean initial density of inflowing particles to the Strait of Juan de Fuca during downwelling-favorable wind stress, influencing the correlation between initial density and wind stress for the Strait of Juan de Fuca experiment (Figure 4i).

4. Discussion

4.1 Effect of wind-driven alongshore shelf currents on inflow source

Alongshore wind stress was highly correlated with initial alongshore position of inflowing particles. This is consistent with previous numerical studies which represented shelf inflow as a vertically-homogenous layer (Beardsley and Hart, 1978; Masse, 1990; Brasseale and MacCready, 2021). During upwelling-favorable wind stress, inflow originated on the Vancouver Island shelf for the Salish Sea and the Washington shelf for the Columbia River estuary. During downwelling-favorable wind stress, inflow originated on the Washington shelf for the Salish Sea and the Oregon shelf for the Columbia River estuary. The consistency of the upwind source result across all experiments here demonstrates that the two-layer result dominates the 3D result even in stratified shelves with ambient currents and realistic atmospheric forcing.

The northern CCS is located at a crossroads in the eastern Pacific current system extending from the equator to the subarctic. Summertime upwelling-favorable wind stress carries cold, fresh Pacific Subarctic Upper Water (PSUW) to the northern CCS, and wintertime downwelling-favorable wind stress brings in warm, salty Pacific Equatorial Water (PEW) (Thomson and

Krassovski, 2010). The different properties of PSUW and PEW account for a significant amount of the seasonal variability of northern CCS shelf water (Stone et al., 2018). Despite seasonal variation in shelf source waters, latitudinal variation along 800 km of the northern CCS has been demonstrated to be minimal (Hickey et al., 2016; Stone et al., 2018). Thus, the horizontal direction of shelf inflow in this region is likely to affect the salinity and temperature of shelf inflow when the local wind and current directions reflect the large-scale patterns in the northern CCS.

The alongshore source of inflow is important because biogeochemical water properties such as oxygen are heterogeneously distributed along the shelf and slope. Although the upwelling season is always associated with lower shelf oxygen in this region (Connolly et al., 2010; Siedlecki et al., 2015), shelf inflow sourced from hypoxic hot spots may transport hypoxic waters into estuaries. Estuaries along the Vancouver Island shelf have been observed to be more resistant to hypoxia than along the Washington shelf because of the width of the shelf and the Vancouver Island current (Bianucci et al., 2010). However, the Juan de Fuca eddy, which forms on the northern edge of the Juan de Fuca canyon on the Vancouver Island shelf from spring until fall (Freeland and Denman, 1982; Foreman et al., 2008), is a known hotspot for hypoxia (Crawford and Thomson 1991; Crawford and Peña, 2013; Siedlecki et al., 2015; Sahu et al., 2022). Inflow sourced from the Juan de Fuca eddy may account for the hypoxic inflow to the Salish Sea observed by Feely et al. (2010). Hypoxia is more severe on the Washington shelf than the Oregon shelf (Connolly et al., 2010), which may help explain the source of hypoxic intrusions to the Columbia River estuary observed during upwelling season (Roegner et al., 2011).

311 *4.2 Effect of wind-driven Ekman dynamics on inflow source*

312 The Ekman response on the shelf was expected to avail deeper and denser water to estuaries
313 during upwelling-favorable wind stress, but evidence for Ekman dynamics was mixed. Neither
314 experiment saw an increase in absolute depth of inflow during upwelling-favorable wind stress
315 (Figure 4c–d). Inflow to both the Salish Sea and Columbia River estuary originated from a
316 greater relative depth during upwelling-favorable wind stress (Figure 4e–f), consistent with
317 onshore transport in the bottom boundary layer during upwelling-favorable wind stress predicted
318 by Ekman dynamics. However, the correlation between relative depth and wind stress could be
319 also explained by the greater portion of inflow originating over greater isobaths during
320 downwelling-favorable wind stress (Figure 4g–h). For the Strait of Juan de Fuca, buoyant
321 Columbia River plume intrusions during downwelling-favorable winds (Thomson, 2007;
322 Giddings and MacCready, 2017) near the surface may also partially explain the correlation of
323 relative depth of inflow with wind stress. The correlation between density and wind stress
324 expected from Ekman dynamics was seen in inflow to the Strait of Juan de Fuca (Figure 4i), but
325 it was not seen in the Columbia River estuary (Figure 4j). This discrepancy is hard to explain
326 using Ekman dynamics alone. However, if the correlation between density and wind stress to the
327 Strait of Juan de Fuca was wholly or in part due to Columbia River plume intrusions, this would
328 be consistent with the lack of similar correlation in inflow to the Columbia River estuary. The
329 inconclusive evidence for Ekman dynamics in these results should not be taken to mean that
330 Ekman dynamics are unimportant to northern CCS estuaries, only that Ekman transport was not
331 obviously reflected within the Lagrangian framework represented in particle tracking
332 experiments. Ekman transport may be less apparent in a particle's trajectory than shelf currents
333 because it is slower and only affects a fraction of the water column. Cross-shelf bottom boundary

334 layer currents are slower than shelf currents because they are generated by Coriolis deflection of
335 decelerating along-shelf flow.
336
337 Regardless of the mechanism, inflow originated from the shelf during upwelling and offshore
338 during downwelling. Whether inflow originated on the shelf or offshore has implications for its
339 biogeochemical properties even when absolute source depth does not change. An inflow source
340 from shelf water during upwelling explains observed hypoxic intrusions to both the Salish Sea
341 (Feely et al., 2010) and Columbia River estuary (Roegner et al., 2011) during summertime, as
342 oxygen levels in bottom shelf waters have been observed to be lower than slope waters at the
343 same depth and isopycnal in this region (Crawford and Peña, 2013). The slope source of inflow
344 during downwelling-favorable winds reflects the shoaling of the CUC shoals during winter,
345 availing poleward-flowing slope waters as inflow to northern CCS estuaries (Hickey, 1979;
346 Thomson and Kassovski, 2010; Connolly et al., 2014). Although the shoaled CUC aligns with
347 the direction and of shelf flow in wintertime, slope and shelf currents are dynamically distinct.
348 Shelf flow variation is driven by wind stress directly on a time scale of days or weeks, while
349 slope flow variation is driven by wind stress curl on a time scale of months or years (Hickey,
350 1979). Subsequently, shelf and slope water properties in the northern CCS are not correlated
351 (Stone et al., 2018).
352
353 *4.3 Effect of canyons on inflow source*
354 Since submarine canyons are known to enhance upwelling (Allen and Hickey, 2010; Zhang and
355 Lentz, 2017), it was expected that the Juan de Fuca and Astoria canyons would be paths for deep
356 inflow to reach the Salish Sea and Columbia River estuary respectively during upwelling-

favorable wind stress. The Juan de Fuca canyon was a conduit for inflow to the Strait of Juan de Fuca during all wind stress experiments. Previous studies have observed inflow to the Strait of Juan de Fuca originating from the Juan de Fuca canyon during upwelling-favorable wind conditions (Cannon, 1972; Feely et al., 2010; Alford and MacCready, 2014). Onshore Juan de Fuca canyon flow during downwelling-favorable wind stress does not have precedent in literature. Downwelling-favorable winds were associated with offshore flow through canyons in idealized models (Spurgin and Allen, 2014), realistic models of the neighboring Clayoquot canyon (Howatt et al., 2022), and observations near the Juan de Fuca canyon floor (Cannon, 1972). However, the Juan de Fuca canyon is unique among northern CCS submarine canyons because its canyon head begins in the Strait of Juan de Fuca. In models, canyons that begin in estuary mouths behave as extensions of the estuary, steering estuarine outflow and lengthening the salinity intrusion (Lee and Valle-Levinson, 2013). Other mechanisms such as topographic steering (Kämpf, 2018) and coastal trapped waves (Saldías et al., 2021) could explain upwelling in canyons regardless of wind direction. Further studies, including a dedicated process study using models and additional observations of Juan de Fuca canyon flow during downwelling-favorable winds, would help confirm and explain this result. The Astoria canyon was rarely a conduit for inflow to the Columbia River estuary.

5. Conclusions

The ocean end of the estuary influences the physical and biogeochemical composition of the estuary, but variations in the ocean end due to wind stress are still understudied. This study helps to explain seasonal variability in northern CCS estuaries by supporting the idealized numerical model results of Beardsley and Hart (1978), Masse (1990) and Brasseale and MacCready (2021)

and demonstrating correlation of wind stress with variations in physical inflow properties (density, temperature, salinity). Wind stress was found to be strongly correlated with the initial alongshore position of inflowing particles, such that inflow originated upwind of both the Salish Sea and the Columbia River estuary. Ekman layer transport influenced initial inflowing particle relative depth during upwelling-favorable wind stress releases. During downwelling-favorable wind stress releases, initial particle depth was influenced by Columbia River plume intrusions to the Strait of Juan de Fuca and wintertime shoaling of the CUC over the continental slope. Subsequently, inflowing particles from downwelling-favorable wind stress releases had shallower relative initial depth than their upwelling counterparts. The Juan de Fuca canyon influenced the paths of inflowing particles to the Salish Sea during both upwelling- and downwelling-favorable wind stress releases, despite expectations that onshore canyon flow would only occur during upwelling-favorable wind stress. Contrarily, the Astoria canyon was rarely a source to the Columbia River estuary. Further process studies are needed to understand how large estuaries at canyon heads can influence canyon dynamics.

Data Availability Statement

The hydrodynamic model output used in this study is stored in netCDF format on hard drives at the University of Washington. Model output is available upon request from the corresponding author. The source code for Tracker is hosted on Github at https://github.com/parkermac/LO/tree/v1.1/tracker. The associated Zenodo DOI and data files are at https://doi.org/10.5281/zenodo.7783639.

Acknowledgments

Julie Keister, LuAnne Thompson, and Alexander Horner-Devine provided valuable feedback on the version of this work that appeared in Dr. Brasseale's thesis. Noel Pelland, Melanie Fewings, and Jessica Garwood gave ongoing feedback during revisions. Helpful conversations were also held with Sarah Giddings, Duncan Wheeler, Helen Zhang, and Alex Simpson. This work would not have been possible without David Darr providing essential assistance with the server. This project was funded by the National Science Foundation under grant OCE-1634148.

References

Alford, M.H., and P. MacCready, 2014. Flow and mixing in Juan de Fuca Canyon, Washington. *Geophys. Res. Lett.,* 41, 1608–1615, doi: 10.1002/2013GL058967.

Allen, S.E. and B.M. Hickey, 2010. Dynamics of advection-driven upwelling over a shelf break submarine canyon. *J. Geophys. Res. Oceans.,* 115, C08018, doi: 10.1029/2009JC005731.

Austin, J.A., and J.A. Barth, 2002. Variation in the position of the upwelling front on the Oregon shelf. *J. Geophys. Res. Oceans.* 107 (C11), 3180, doi: 10.1029/2001JC000858.

Banas, N.S., MacCready, P., and B.M. Hickey, 2009. The Columbia River as cross-shelf exporter and along-coast barrier. *Cont. Shelf. Res.*, 29, 292–301, doi: 10.1016/j.csr.2008.03.011.

Beardsley, R.C. and J. Hart, 1978. A simple theoretical model for the flow of an estuary onto a continental shelf. *J. Geophys. Res.*, 83 (C2), 873–883, doi: 0148-0227/78/027C-0842503.00.

Bianucci, L., Denman, K.L., and D. Ianson, 2010. Low oxygen and high inorganic carbon on the Vancouver Island Shelf. *J. Geophys Res. Oceans*, 116, C07011, doi: 10.1029/2010JC006720.

426 Brasseale, E.A., Grason, E.W., McDonald, P.S., Adams, J., and P. MacCready, 2019. Larval
427 transport modeling support for identifying population sources of European Green Crab in
428 the Salish Sea. *Estuar. Coasts.*, 42 (6), 1586–1599, doi: 10.1007/s12237-019-00586-2.
429 Brasseale, E., and P. MacCready, 2021. Shelf sources of estuarine inflow. *J. Phys. Oceanogr.*,
430 51, doi: 10.1175/JPO-D-20-0080.1.
431 Cannon, G.A., 1972. Wind effects on currents observed in Juan de Fuca submarine canyon. *J.*
432 *Phys. Oceanogr.*, 2 (3), 281–285, doi: 10.1175/1520-
433 0485(1972)002<0281:WEOCOI>2.0.CO;2.
434 Connolly, T.P., Hickey, B.M., Geier, S.L., and W.P. Cochlan, 2010. Processes influencing
435 seasonal hypoxia in the northern California Current System. *J. Geophys. Res. Oceans.*,
436 115, C03021, doi: 10.1029/2009JC005283.
437 Connolly, T.P., Hickey, B.M., Shulman, I., and R.E. Thomson, 2014. Coastal trapped waves,
438 alongshore pressure gradients, and the California Undercurrent. *J. Phys. Oceanogr.*, 44,
439 319–342, doi: 10.1175/JPO-D-13-095.1.
440 Crawford, W.R., and R.E. Thomson, 1991. Physical oceanography of the western Canadian
441 continental shelf. *Cont. Shelf. Res.*, 11 (8–10), 669–683, doi: 10.1016/0278-
442 4343(91)90073-F.
443 Crawford, W.R., and M.A. Peña, 2013. Declining oxygen on the British Columbia continental
444 shelf. *Atmos. Ocean*, 51 (1), 88–103, doi: 10.1080/07055900.2012.753028.
445 Feely, R.A., et al., 2010. The combined effects of ocean acidification, mixing, and respiration on
446 pH and carbonate saturation in an urbanized estuary. *Estuar. Coast. Shelf S.*, 88, 442–
447 449, doi: 10.1016/j.ecss.2010.05.004.

448 Freeland, H.J., and K.L. Denman, 1982. A topographically controlled upwelling center off
449 southern Vancouver Island. *J. Mar. Res.*, 40 (4), 1069–1093.
450 Foreman, H.J., et al., 2008. Modeling the generation of the Juan de Fuca eddy, *J. Geophys. Res.*,
451 113, C03006, doi: 10.1029/2006JC004082.
452 Giddings, S.N., et al., 2014. Hindcasts of potential harmful algal bloom transport pathways on
453 the Pacific Northwest coast. *J. Geophys. Res. Ocean.*, 119 (4), 2439–2461, doi:
454 10.1002/2013JC009622.
455 Giddings, S.N., and P. MacCready, 2017. Reverse estuarine circulation due to local and remote
456 wind forcing, enhanced by the presence of along-coast estuaries. *J. Geophys. Res.*
457 *Ocean.*, 122 (12), 10184–10205, doi: 10.1002/2016JC012479.
458 Hickey, B.M., 1979. The California current system—hypotheses and facts. *Prog. Oceanogr.*, 8
459 (4), 191–279, doi: 10.1016/0079-6611(79)90002-8.
460 Hickey, B.M., Zhang, X., and N.S. Banas, 2002. Coupling between the California Current
461 System and a coastal plain estuary in low riverflow conditions. *J. Geophys. Res. Ocean.*,
462 107 (C10), 3166, doi: 10.1029/1999JC000160.
463 Hickey, B.M., and N.S. Banas, 2003. Oceanography of the U.S. Pacific Northwest coastal ocean
464 and estuaries with application to coastal ecology. *Estuar.*, 26 (4B), 1010–1031, doi:
465 10.1007/BF02803360.
466 Hickey, B.M., Geier, S., Kachel, N., Ramp, S., Kosro, P.M., and T. Connolly, 2016. Alongcoast
467 structure and interannual variability of seasonal midshelf water properties and velocity in
468 the Northern California Current System. *J. Geophys. Res. Ocean*, 121, 7408–7430, doi:
469 10.1002/2015JC011424.

Howatt, T., Ross, T., and S. Waterman, 2022. Canyon downwelling and water mass influences on winter zooplankton distributions in the coastal Northeast Pacific. *J. Geophys. Res. Ocean.*, 127, e2022JC018540, doi: 10.1029/2022JC018540.

Kämpf, J., 2018. On the dynamics of canyon-flow interactions. *J. Mar. Sci. Eng.*, 6 (129), doi: 10.3390/jmse6040129.

Lee, J., and A. Valle-Levinson, 2013. Bathymetric effects on estuarine plume dynamics. *J. Geophys. Res. Ocean.*, 118 (4), 1969–1981, doi: 10.1002/jgrc.20119.

MacCready, P., et al., 2021. Estuarine circulation, mixing, and residence times in the Salish Sea. *J. Geophys. Res. Ocean.*, 126 (2), e2020JC016738, doi: 10.1029/2020JC016738.

Masse, A.K., 1990. Withdrawal of shelf water into an estuary: a barotropic model. *J. Geophys. Res. Ocean.*, 95 (C9), 16085–16096, doi: 10.1029/JC095iC09p16085.

McLaskey, A.K., et al., 2016. Development of *Euphasia pacifica* (krill) larvae is impaired under pCO_2 levels currently observed in the Northeast Pacific. *Mar. Ecol. Prog. Ser.*, 555, 65–78, doi: 10.3354/meps11839.

Roegner, G.C., Needoba, J.A., and A.M. Baptista, 2011. Coastal upwelling supplies oxygen-depleted water to the Columbia River Estuary. *PLoS ONE*, 6 (4), e18672, doi: 10.1371/journal.pone.0018672.

Sahu, S., et al., 2022. Spatial and temporal origins of the La Perouse low oxygen pool: a combined Lagrangian statistical approach. *J. Geophys. Res. Ocean.*, 127, e2021JC018135, doi: 10.1029/2021JC018135.

Saldías, G.S., Ramos-Musalem, K., and S.E. Allen, 2021. Circulation and upwelling induced by coastal trapped waves over a submarine canyon in an idealized eastern boundary margin. *Geophys. Res. Lett*., 48, e2021GL093548, doi: 10.1029/2021GL093548.

493 Shchepetkin, A.F., and J.C. McWilliams, 2005. The regional oceanic modeling system (ROMS):
494 a split-explicit, free-surface, topography-following-coordinate oceanic model. *Ocean*
495 *Model.*, 9, 347–404, doi: 10.1016/j.ocemod.2004.08.002.
496 Siedlecki, S.A., et al., 2015. Seasonal and interannual oxygen variability on the Washington and
497 Oregon continental shelves. *J. Geophys. Res. Ocean.*, 120, 608–633, doi:
498 10.1002/2014JC010254.
499 Spurgin, J.M., and S.E. Allen, 2014. Flow dynamics around downwelling submarine canyons.
500 *Ocean Sci.*, 10, 799–819, doi: 10.5194/os-10-799-2014.
501 Stone, H.B., Banas, N.S., and P. MacCready, 2018. The effect of alongcoast advection on Pacific
502 Northwest shelf and slope water properties in relation to upwelling variability. *J.*
503 *Geophys. Res. Ocean.*, 123, doi: 10.1002/2017JC013174.
504 Thomson, R.E., Mih-Ly, S.F., and E.A. Kulikov, 2007. Estuarine versus transient flow regimes
505 in Juan de Fuca Strait. *J. Geophys. Res. Ocean.*, 112, C09022, doi:
506 10.1029/2006JC003925.
507 Thomson, R.E., and M.V. Krassovski, 2010. Poleward reach of the California undercurrent
508 extension. *J. Geophys. Res. Ocean*., 115, C09027, doi: 10.1029/2010JC006280.
509 Visser, A., 1997. Using random walk models to simulate the vertical distribution of particles in a
510 turbulent water column. *Mar. Ecol. Prog. Ser.*, 158 (1), 275–281, doi:
511 10.3354/meps158275.
512 Xiong, J. and P. MacCready, 2023. Intercomparisons of five ocean particle tracking software
513 packages. *Geosci. Model Dev. Discuss.* [preprint], doi:10.5194/gmd-2023-45. In review.

514 Zhang, W., and S.J. Lentz, 2017. Wind-driven circulation in a shelf valley. Part 1: Mechanism of
515 the asymmetrical response to along-shelf winds in opposite directions. *J. Phys.*
516 *Oceanogr.*, 47, 2927–2947, doi: 10.1175/JPO-D-17-0083.1.
517

Figure 1: Release points of particles tracked to identify inflow to a) the Strait of Juan de Fuca, and b) the Columbia River estuary. Particles were released at 15-m intervals in the water column for the Strait of Juan de Fuca and 30-m intervals for the Columbia River estuary. Release points are colored by source identification (purple = Vancouver Island shelf, orange = Washington shelf, green = Oregon shelf, gray = offshore of shelf). Yellow diamond = location of wind stress extraction used to calculate $\overline{\tau_y}$. Contour is 200-m isobath.

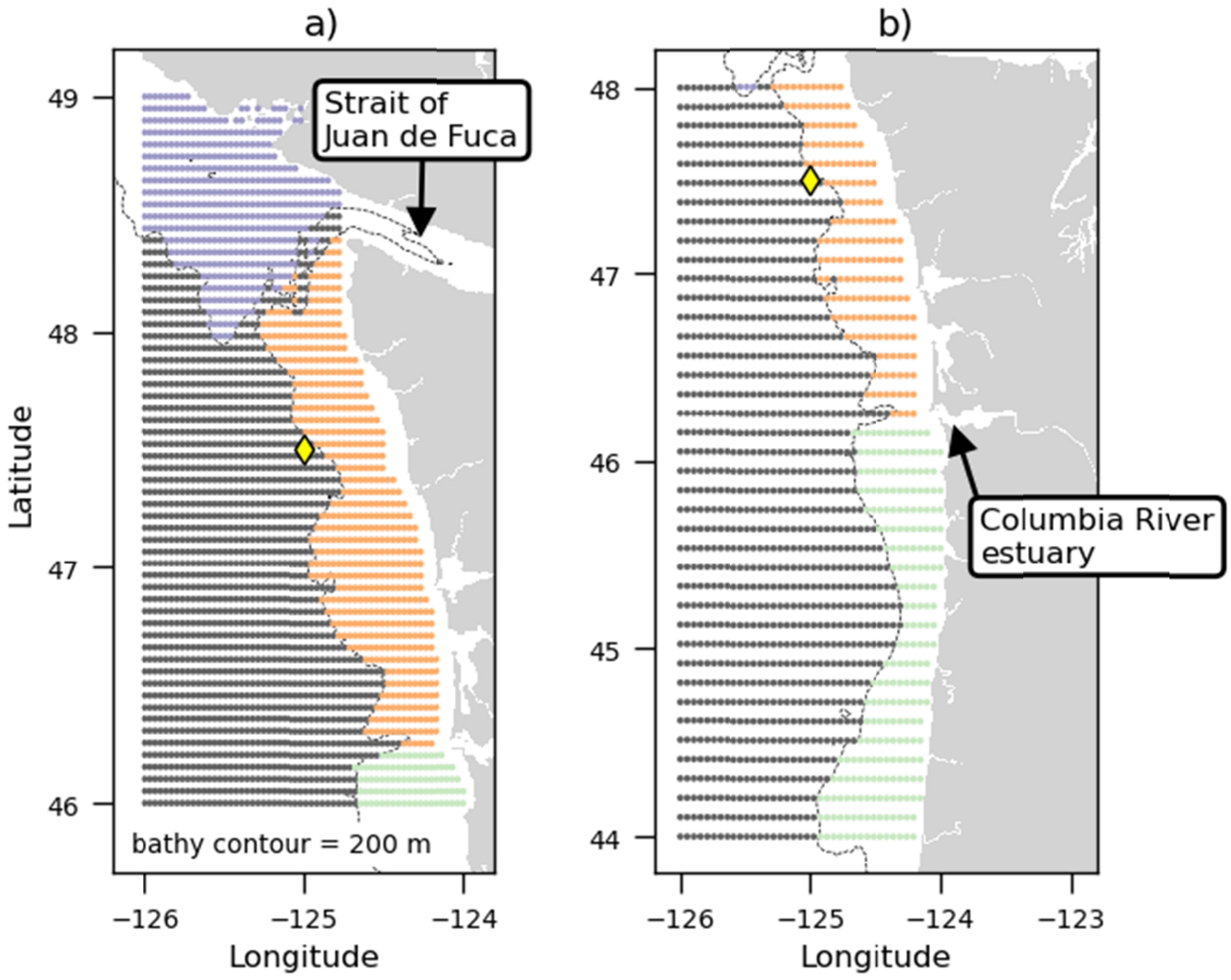

Figure 2: North-south wind stress filtered with a weighted 8-day filter as a proxy for the shelf Ekman response (Austin-Barth, 2002) from Jan 1, 2017 to Jan 1, 2018 extracted from model at location of yellow diamond (Lat: 47.5°, Lon: -125°) in Figure 1. Blue fill behind time series illustrates the timing of the typical upwelling season for this region estimated using the sign of the average of wind stress observed from 2003-2020 at the nearby Cape Elizabeth mooring (lat: 47.35°, lon: -124.73°, NDBC 46041), filtered with same weighted 8-day filter.

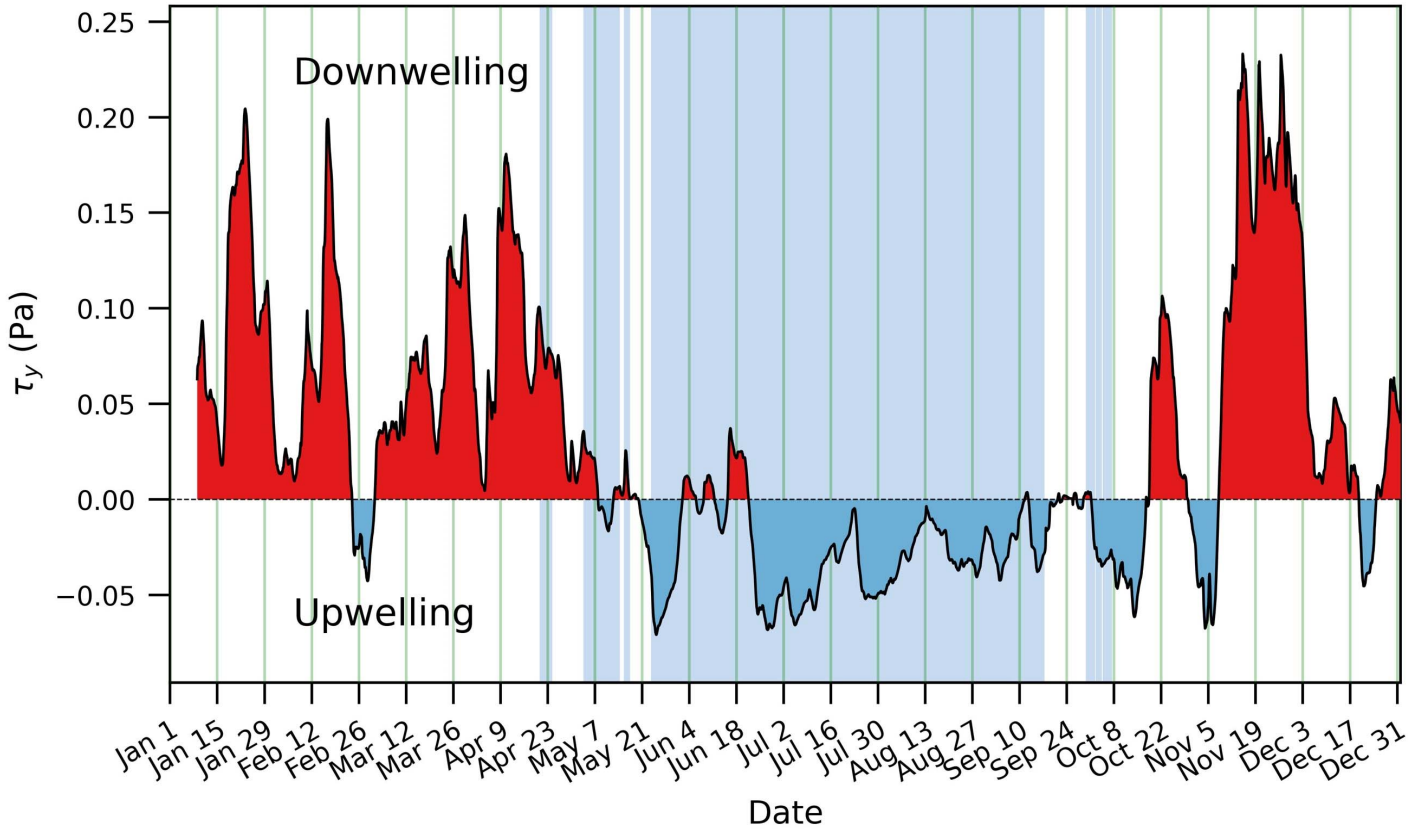

Figure 3: Number of inflowing particles to b) Strait of Juan de Fuca and c) Columbia River estuary per release from each source water region (colors same as Figure 1). Releases are sorted along x-axis by mean wind stress during release (a).

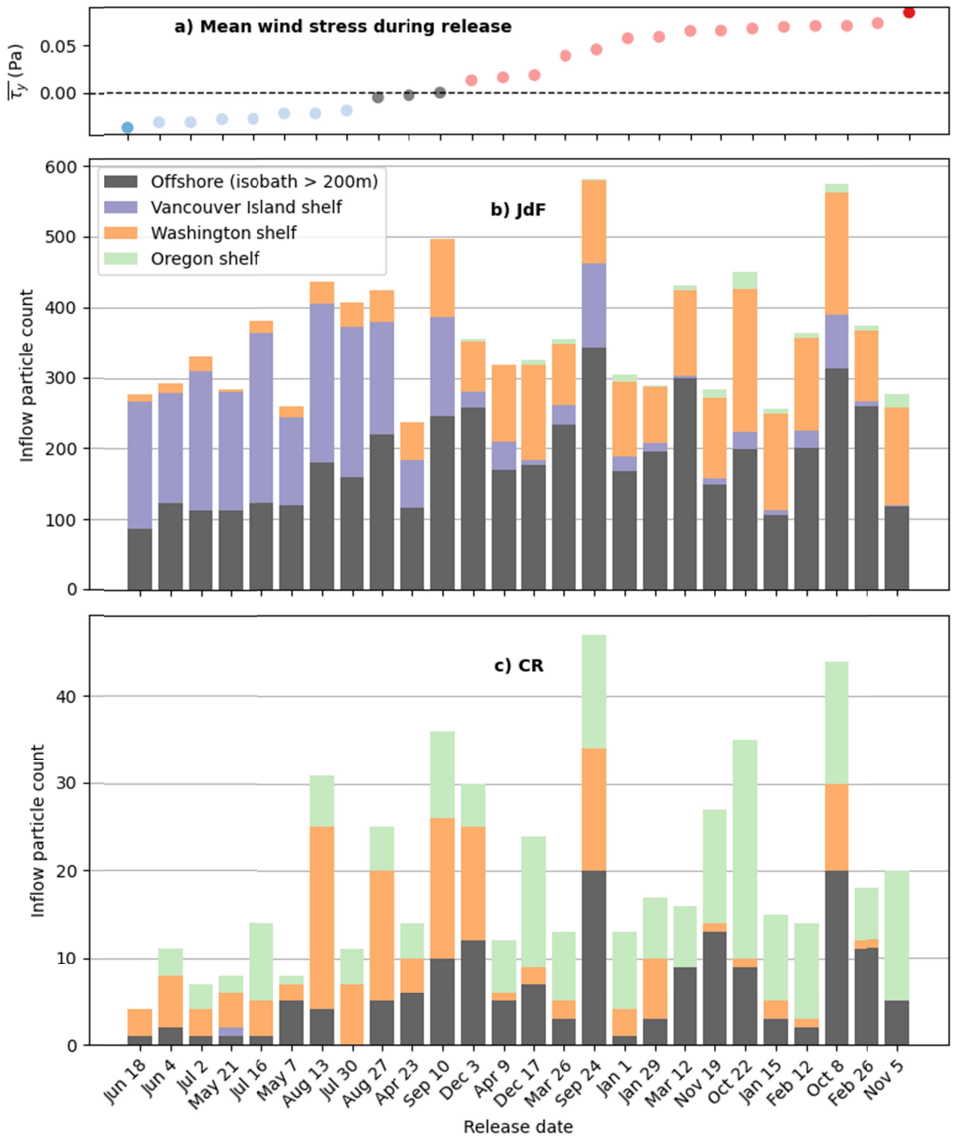

Figure 4: Mean initial positions described in four variables (rows; N-S distance from mouth (km), vertical position (m), and relative vertical position) of inflow to the two estuaries (columns; Strait of Juan de Fuca, Columbia River estuary) as a function of mean N-S wind stress. Releases with downwelling-favorable mean wind stress ($\overline{\tau_y}$ > 0.01 Pa) are red, releases with upwelling-favorable mean wind stress ($\overline{\tau_y}$ < –0.01 Pa) are blue, and releases with near zero mean wind stress (–0.01< $\overline{\tau_y}$ <0.01) are gray. Darker markers are used for releases with greatest mean upwelling- and downwelling-favorable wind stresses (June 18 and November 5, respectively). Error bars show the 25th percentile to the 75th percentile of particle initial positions and hourly wind stresses for each release. Darker gray dashed line indicates the best linear fit to the mean initial positions for each variable/experiment plot. Correlation coefficients (R^2) are printed in each plot. Wind stress $\overline{\tau_y}$=0 is indicated with a lighter gray dashed line.

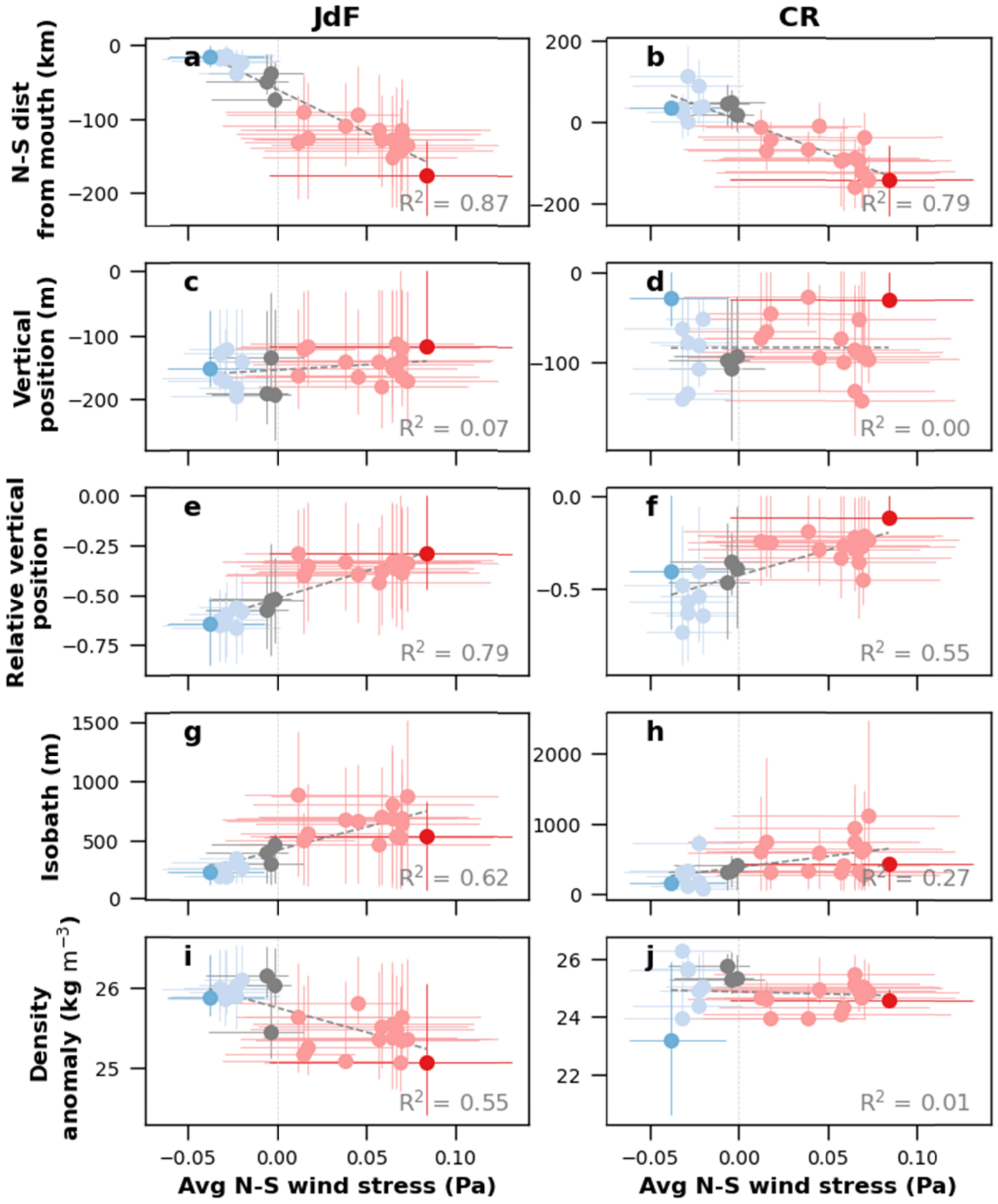
JdF
CR
N-S dist from mouth (km)
Vertical position (m)
Relative vertical position
Isobath (m)
Density anomaly (kg m^{-3})
a
b
c
d
e
f
g
h
i
j
R^2 = 0.87
R^2 = 0.79
R^2 = 0.07
R^2 = 0.00
R^2 = 0.79
R^2 = 0.55
R^2 = 0.62
R^2 = 0.27
R^2 = 0.55
R^2 = 0.01
Avg N-S wind stress (Pa)
Avg N-S wind stress (Pa)

551

552 Figure 5: Summary of particles inflowing to the Strait of Juan de Fuca during upwelling-
553 favorable wind stress conditions. Only particle tracks found east of magenta line were classified
554 as "inflow." Top subplots depict 2D histograms of initial positions of inflowing particles from all
555 upwelling releases plotted in (a) plan view and (b) profile. In profile plot, an example
556 bathymetric transect is plotted from the shelf where most particles are sourced (solid black line)
557 and along the Juan de Fuca canyon (dashed black line). Bottom subplots (c,d) depict tidally-
558 smoothed tracks of inflowing particles from an example release (circles=initial positions). One
559 representative particle track is highlighted with a thicker, darker line.

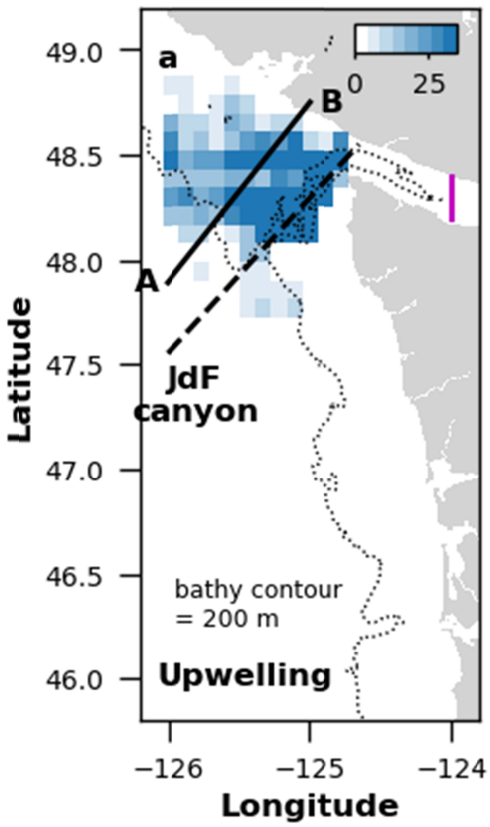
a
0
25
B
A
JdF
canyon
bathy contour
= 200 m
Upwelling
49.0
48.5
48.0
47.5
47.0
46.5
46.0
Latitude
−126
−125
−124
Longitude

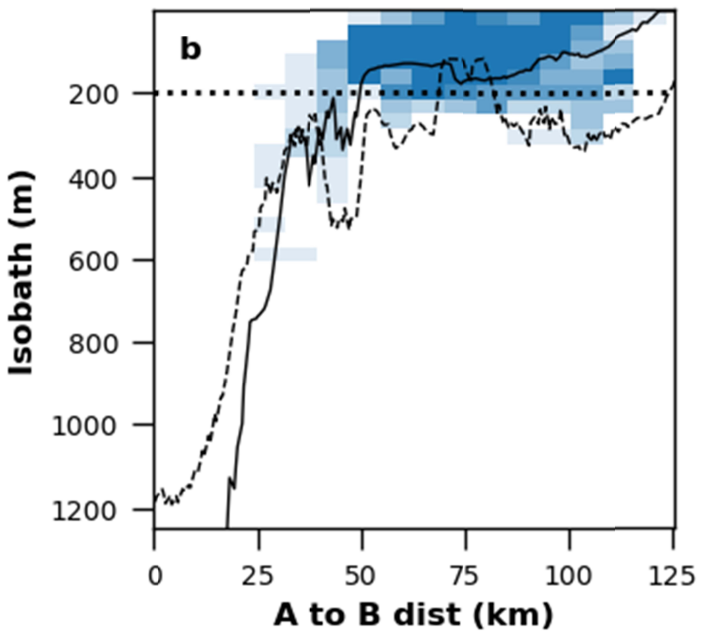
b
200
400
600
800
1000
1200
Isobath (m)
0
25
50
75
100
125
A to B dist (km)

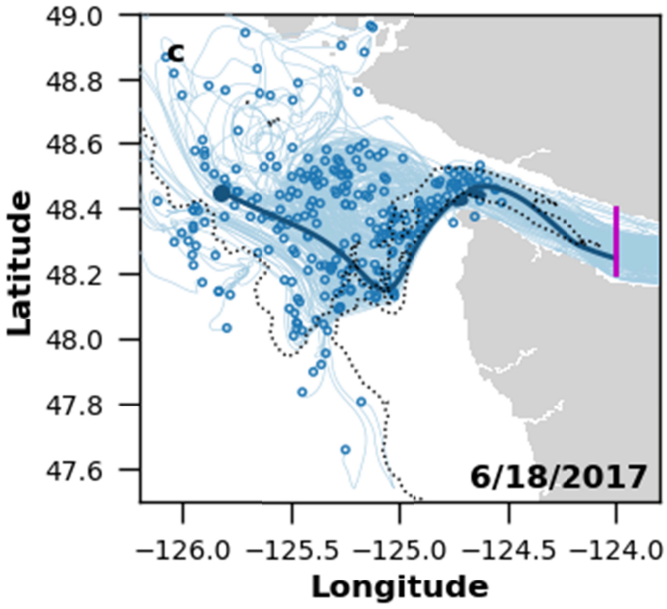
c
49.0
48.8
48.6
48.4
48.2
48.0
47.8
47.6
Latitude
6/18/2017
−126.0
−125.5
−125.0
−124.5
−124.0
Longitude

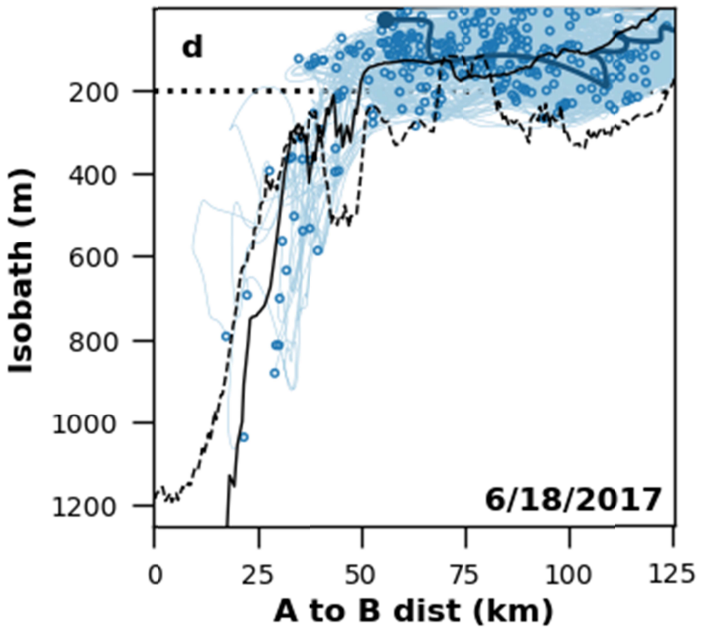
d
200
400
600
800
1000
1200
Isobath (m)
6/18/2017
0
25
50
75
100
125
A to B dist (km)

560

561 Figure 6: As for Figure 5, but for downwelling favorable wind.

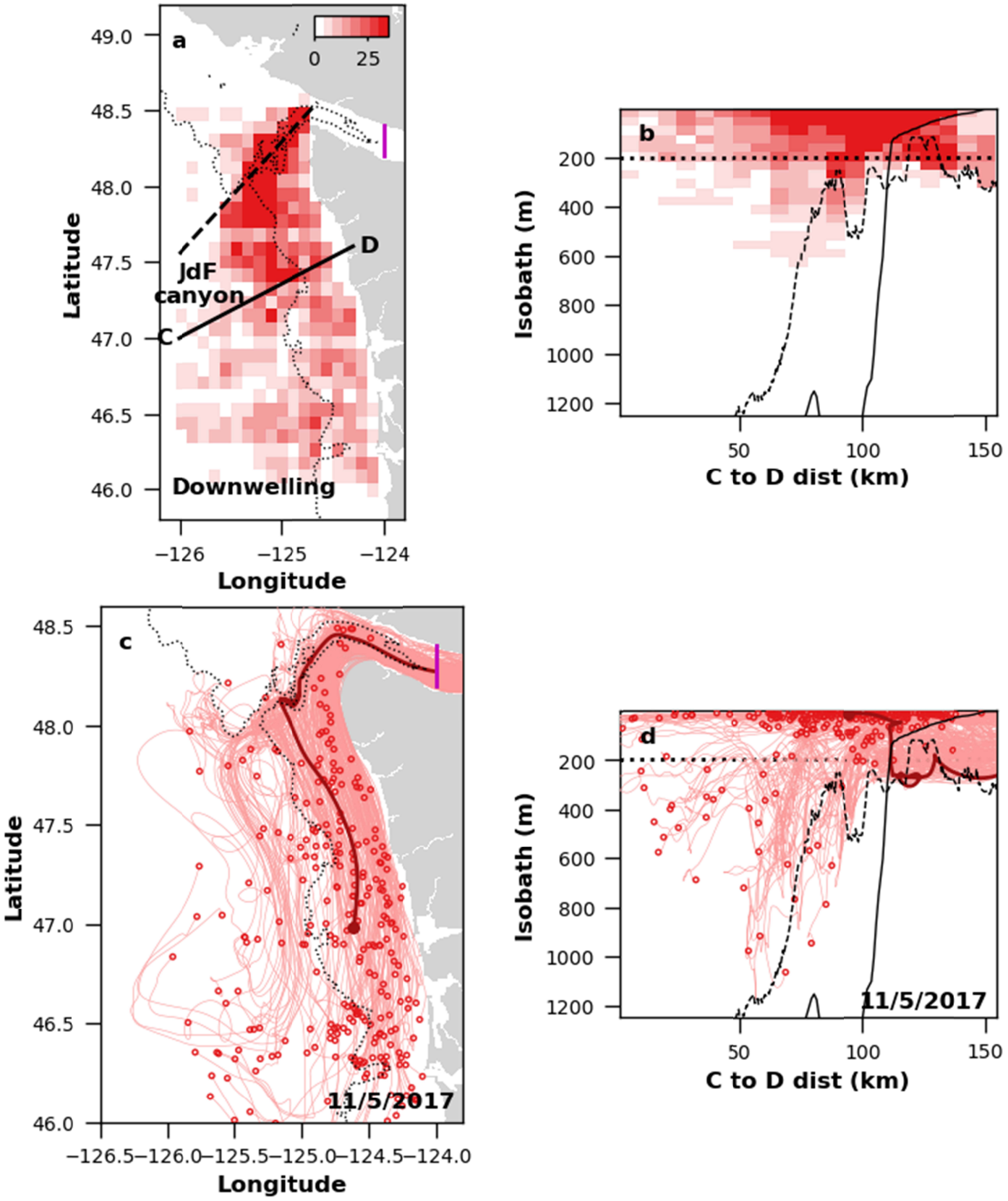
a
0
25
49.0
48.5
48.0
47.5
47.0
46.5
46.0
Latitude
JdF
canyon
C
D
Downwelling
−126
−125
−124
Longitude
b
200
400
600
800
1000
1200
Isobath (m)
50
100
150
C to D dist (km)
c
48.5
48.0
47.5
47.0
46.5
46.0
Latitude
11/5/2017
−126.5
−126.0
−125.5
−125.0
−124.5
−124.0
Longitude
d
200
400
600
800
1000
1200
Isobath (m)
11/5/2017
50
100
150
C to D dist (km)

562

563 Figure 7: As Figure 5, but for Columbia River estuary under upwelling-favorable wind stress,

564 and with no canyon bathymetry transect in profile plots.

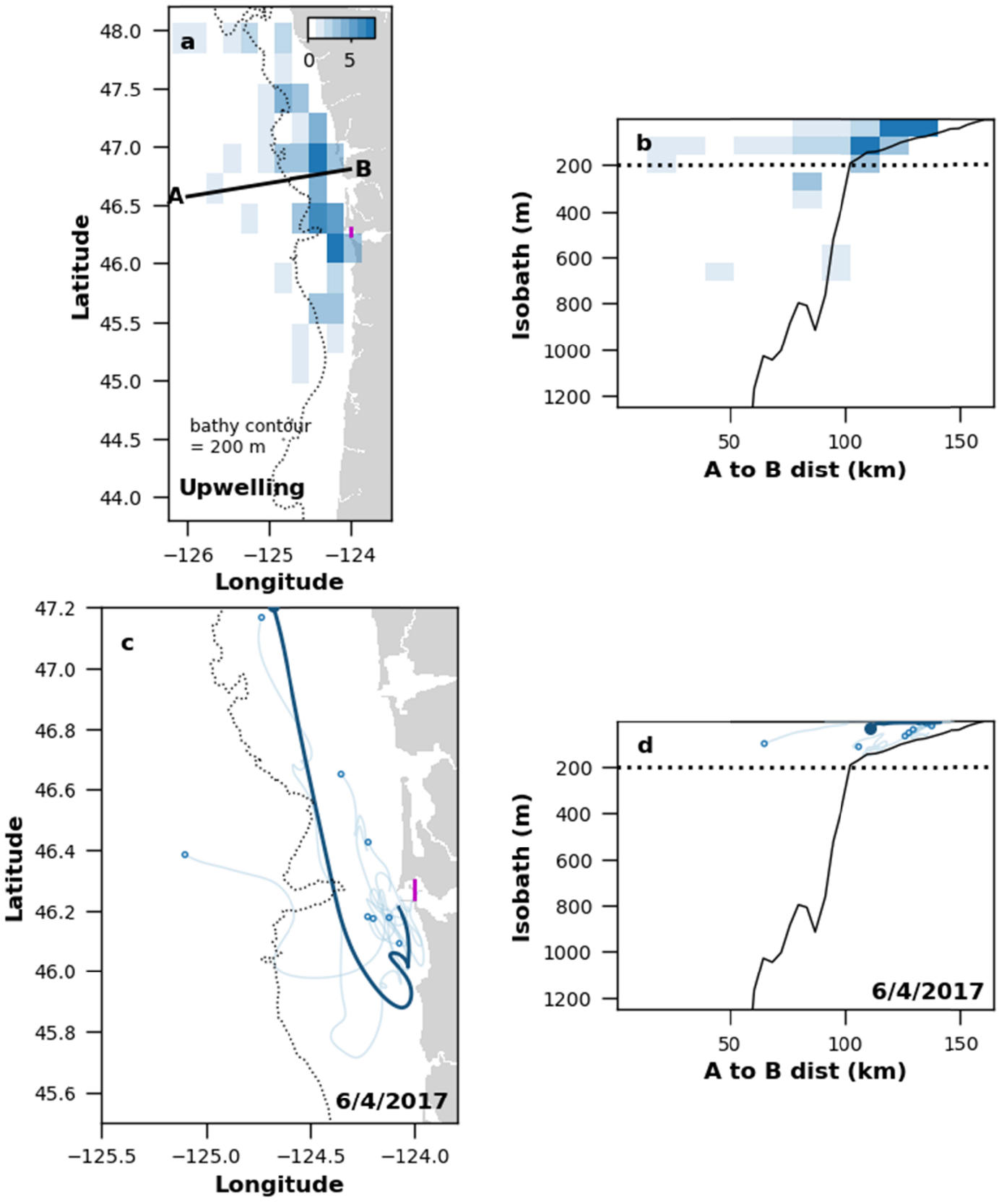
a
0
5
A
B
bathy contour
= 200 m
Upwelling
Latitude
Longitude
48.0
47.5
47.0
46.5
46.0
45.5
45.0
44.5
44.0
−126
−125
−124
b
Isobath (m)
A to B dist (km)
200
400
600
800
1000
1200
50
100
150
c
6/4/2017
Latitude
Longitude
47.2
47.0
46.8
46.6
46.4
46.2
46.0
45.8
45.6
−125.5
−125.0
−124.5
−124.0
d
6/4/2017
Isobath (m)
A to B dist (km)

565

566 Figure 8: As Figure 5, but for Columbia River estuary under downwelling-favorable wind stress.

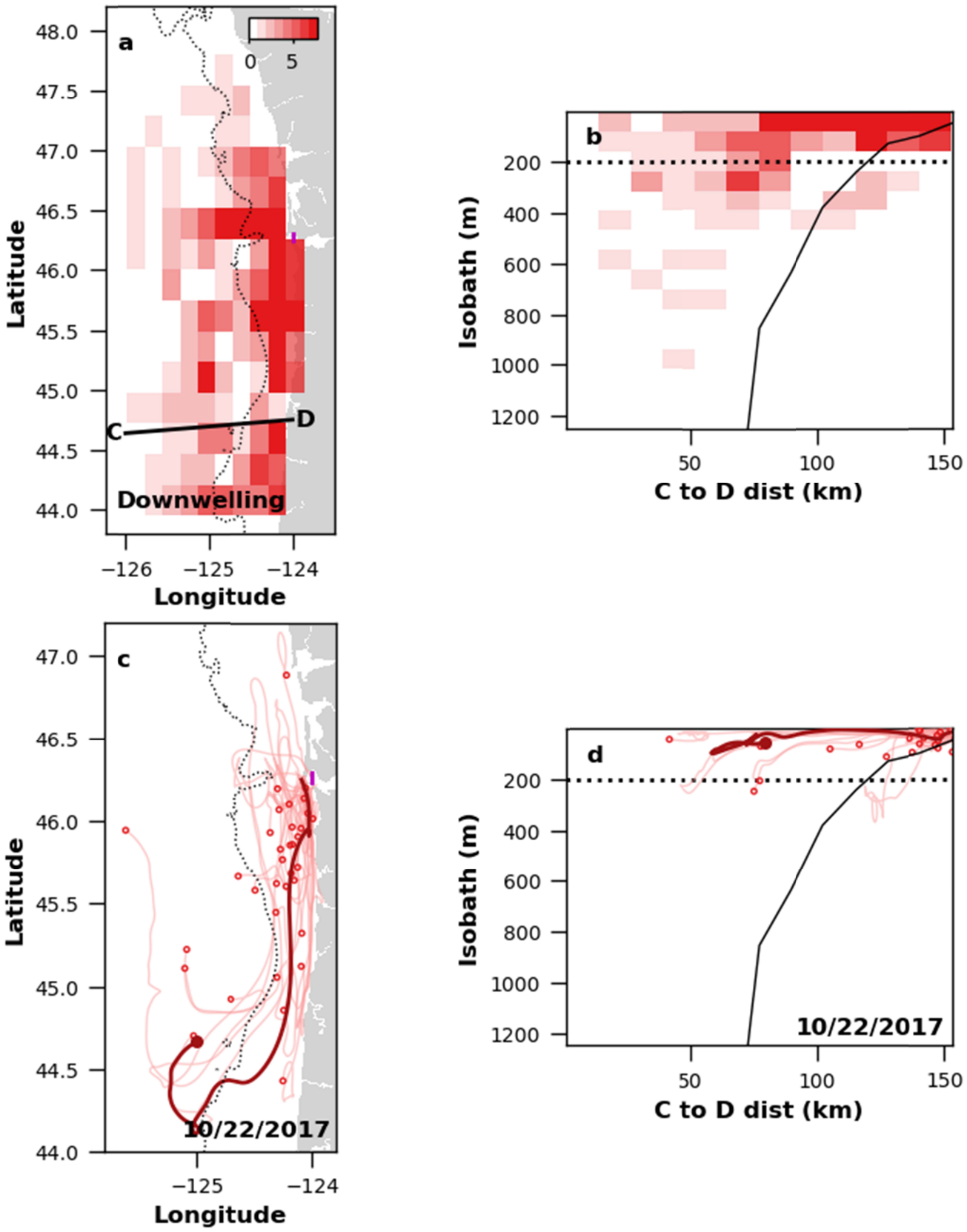
a
0
5
48.0
47.5
47.0
46.5
46.0
45.5
45.0
44.5
44.0
Latitude
C
D
Downwelling
−126
−125
−124
Longitude
b
200
400
600
800
1000
1200
Isobath (m)
50
100
150
C to D dist (km)
c
47.0
46.5
46.0
45.5
45.0
44.5
44.0
Latitude
10/22/2017
−125
−124
Longitude
d
200
400
600
800
1000
1200
Isobath (m)
10/22/2017
50
100
150
C to D dist (km)

567

Figure 9: Initial temperature-salinity distributions for shelf particles that flowed into a) the Strait of Juan de Fuca, and b) the Columbia River estuary. Points are colored by the mean wind stress for the release. Red diamond markers indicate downwelling-favorable mean wind stress ($\overline{\tau_y}$ > 0.01 Pa), and blue circles upwelling-favorable mean wind stress ($\overline{\tau_y}$ < –0.01 Pa). Darker and larger markers are used for the releases with the greatest mean downwelling- and upwelling-favorable wind stresses (11/5/2017 and 6/18/2017, respectively). Releases with mean wind stress –0.01< $\overline{\tau_y}$ <0.01 were omitted. Gray contours are density anomaly (g kg^{-1}).

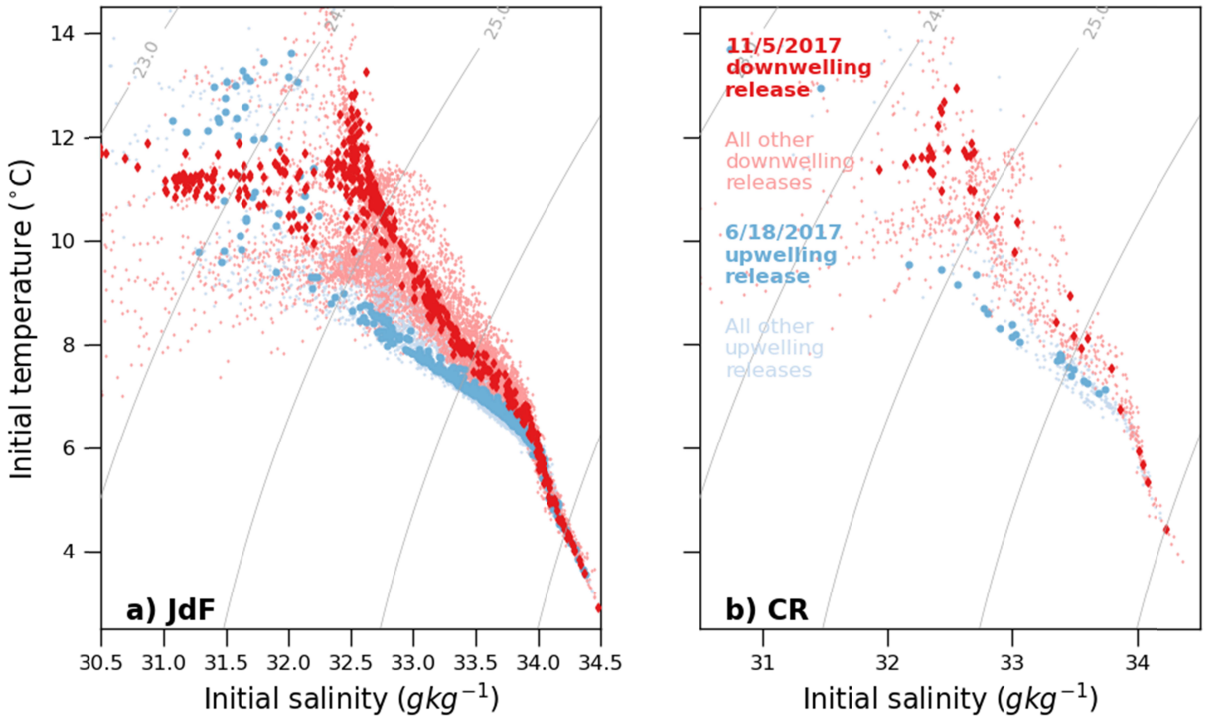

Figure 1.

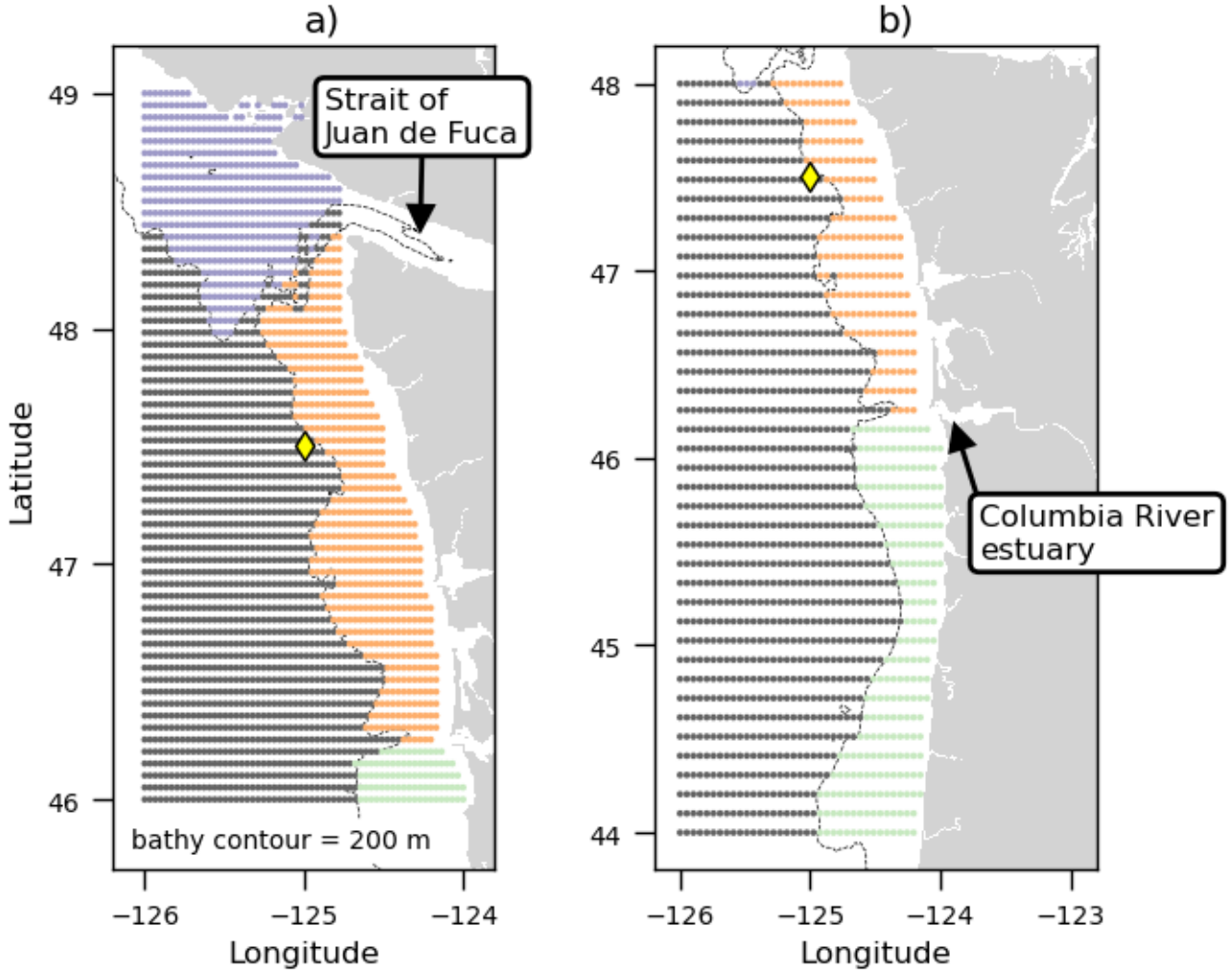
a)
b)
Strait of
Juan de Fuca
Columbia River
estuary
bathy contour = 200 m
Latitude
Longitude
49
48
47
46
44
−126
−125
−124
−123

Figure 2.

Downwelling

Upwelling

τ_y (Pa)

0.25
0.20
0.15
0.10
0.05
0.00
−0.05

Jan 1
Jan 15
Jan 29
Feb 12
Feb 26
Mar 12
Mar 26
Apr 9
Apr 23
May 7
May 21
Jun 4
Jun 18
Jul 2
Jul 16
Jul 30
Aug 13
Aug 27
Sep 10
Sep 24
Oct 8
Oct 22
Nov 5
Nov 19
Dec 3
Dec 17
Dec 31

Date

Figure 3.

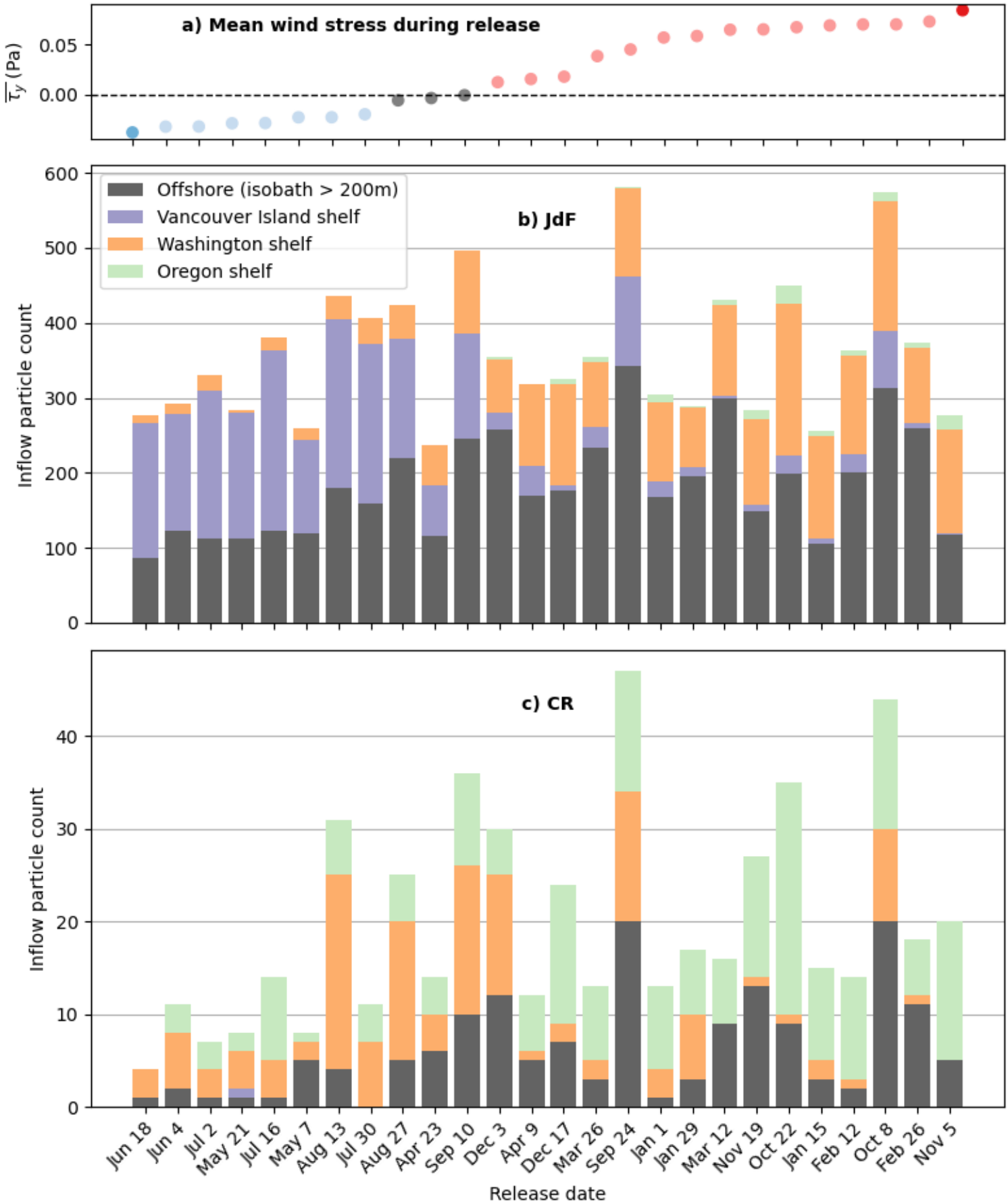
a) Mean wind stress during release
$\overline{\tau_y}$ (Pa)
0.05
0.00
b) JdF
Offshore (isobath > 200m)
Vancouver Island shelf
Washington shelf
Oregon shelf
Inflow particle count
600
500
400
300
200
100
0
c) CR
Inflow particle count
40
30
20
10
0
Jun 18
Jun 4
Jul 2
May 21
Jul 16
May 7
Aug 13
Jul 30
Aug 27
Apr 23
Sep 10
Dec 3
Apr 9
Dec 17
Mar 26
Sep 24
Jan 1
Jan 29
Mar 12
Nov 19
Oct 22
Jan 15
Feb 12
Oct 8
Feb 26
Nov 5
Release date

Figure 4.

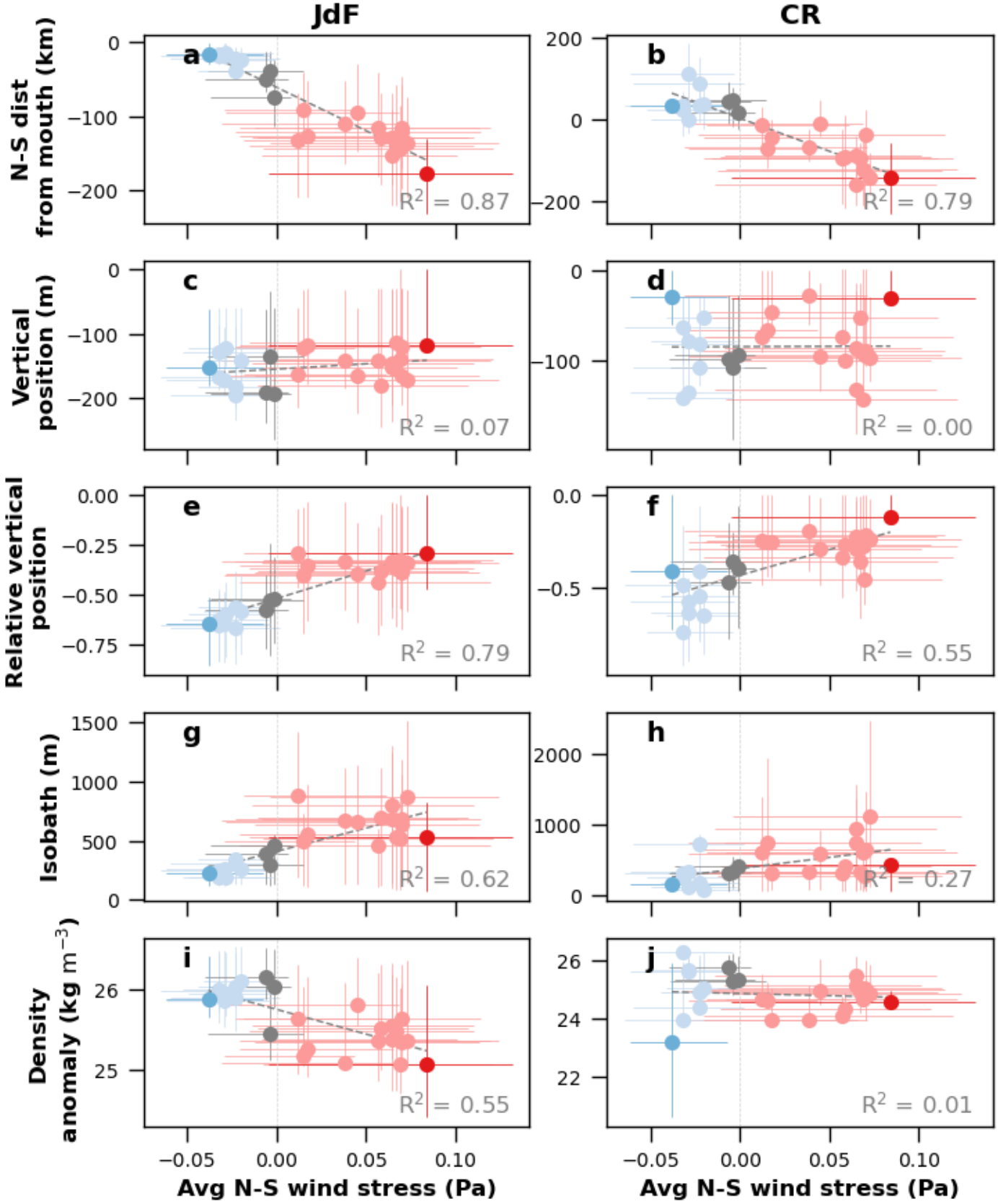
JdF
CR
N-S dist from mouth (km)
Vertical position (m)
Relative vertical position
Isobath (m)
Density anomaly (kg m^{-3})
a
b
c
d
e
f
g
h
i
j
R^2 = 0.87
R^2 = 0.79
R^2 = 0.07
R^2 = 0.00
R^2 = 0.79
R^2 = 0.55
R^2 = 0.62
R^2 = 0.27
R^2 = 0.55
R^2 = 0.01
0
−100
−200
200
0
−200
0
−100
−200
0
−100
0.00
−0.25
−0.50
−0.75
0.0
−0.5
1500
1000
500
0
2000
1000
0
26
25
26
24
22
−0.05
0.00
0.05
0.10
Avg N-S wind stress (Pa)
Avg N-S wind stress (Pa)

Figure 5.

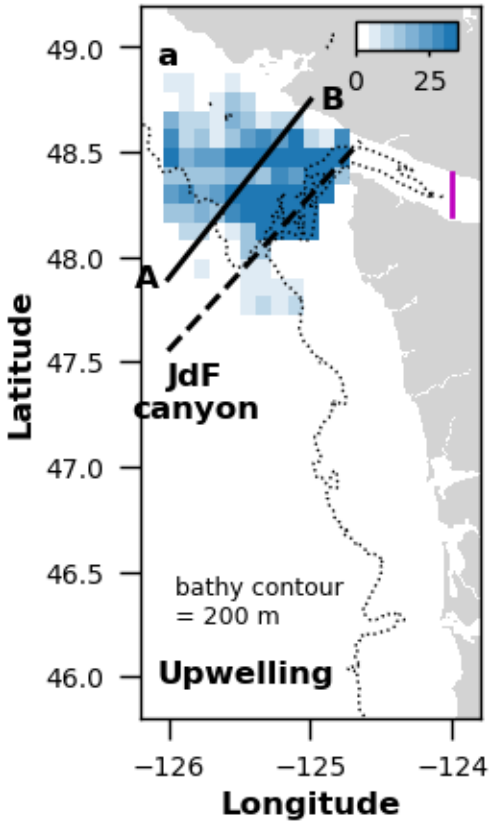
a
0
25
B
A
JdF
canyon
bathy contour
= 200 m
Upwelling
49.0
48.5
48.0
47.5
47.0
46.5
46.0
Latitude
−126
−125
−124
Longitude

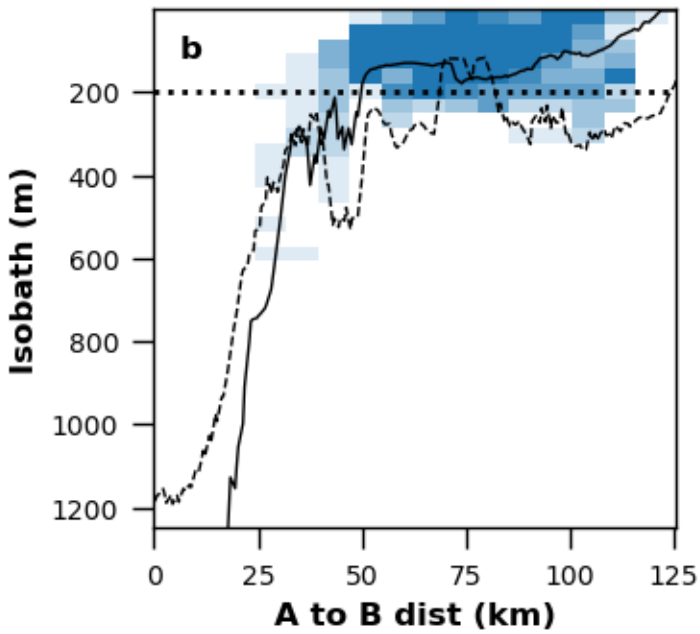
b
200
400
600
800
1000
1200
Isobath (m)
0
25
50
75
100
125
A to B dist (km)

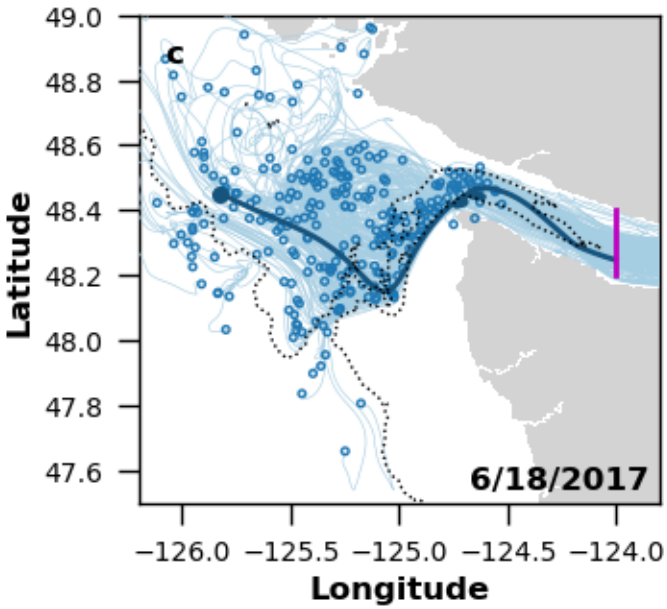
c
49.0
48.8
48.6
48.4
48.2
48.0
47.8
47.6
Latitude
6/18/2017
−126.0
−125.5
−125.0
−124.5
−124.0
Longitude

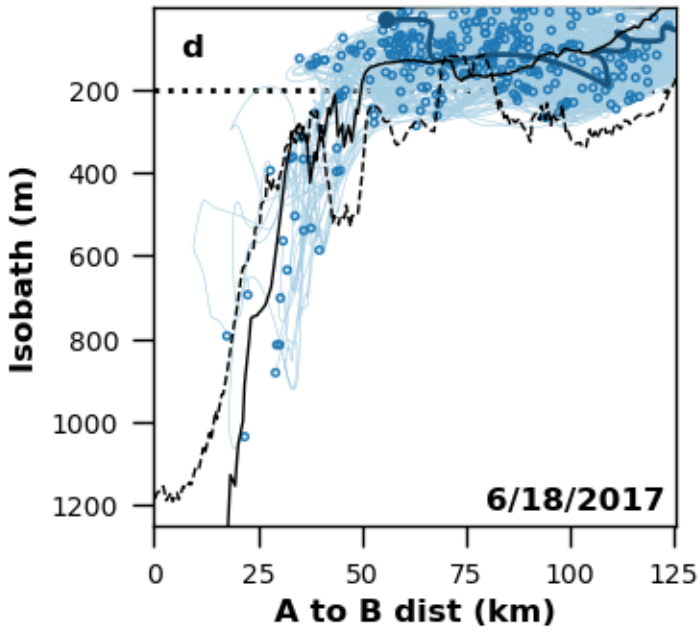
d
200
400
600
800
1000
1200
Isobath (m)
6/18/2017
0
25
50
75
100
125
A to B dist (km)

Figure 6.

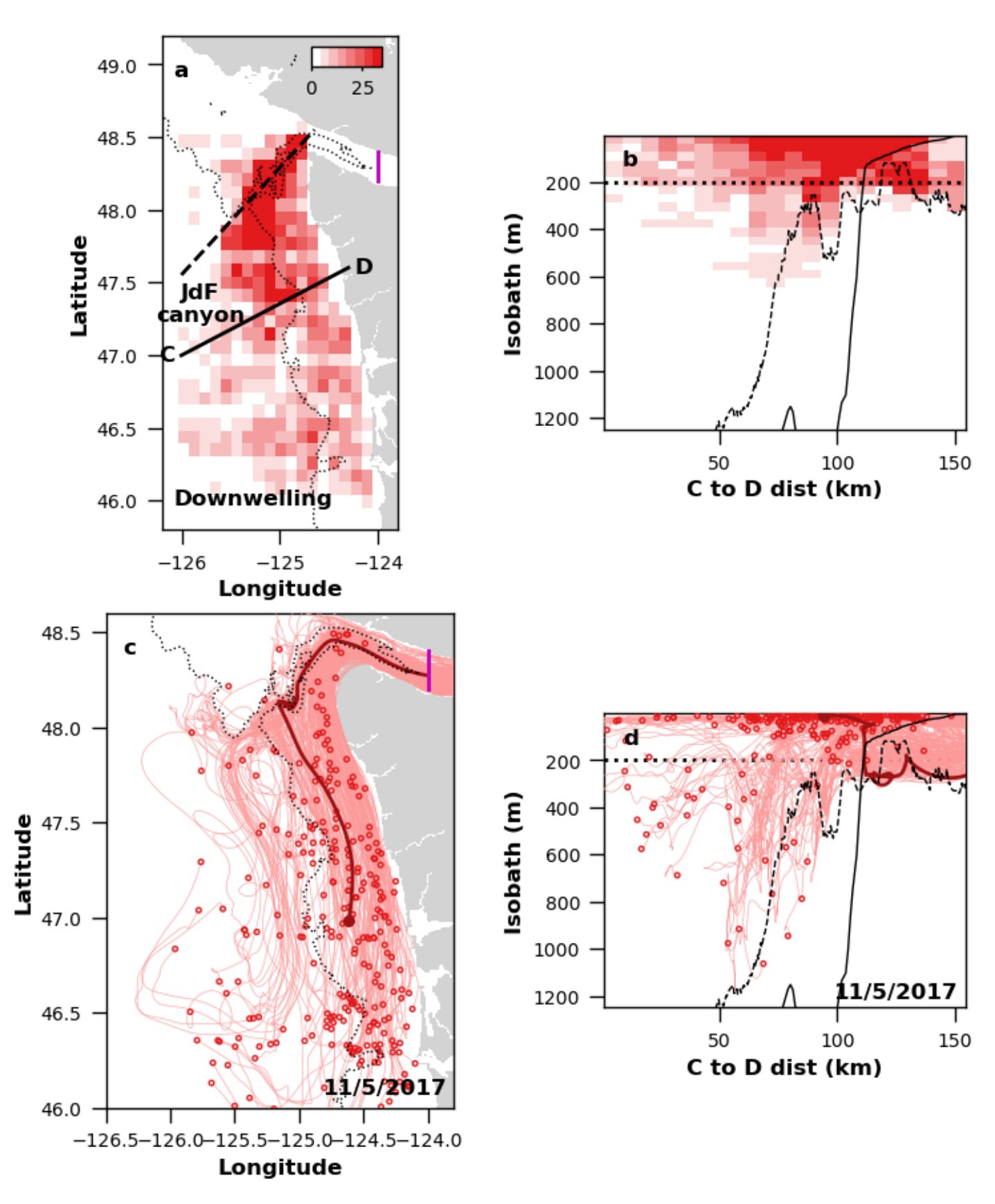
a
0
25
49.0
48.5
48.0
47.5
47.0
46.5
46.0
Latitude
JdF
canyon
C
D
Downwelling
−126
−125
−124
Longitude
b
200
400
600
800
1000
1200
Isobath (m)
50
100
150
C to D dist (km)
c
48.5
48.0
47.5
47.0
46.5
46.0
Latitude
11/5/2017
−126.5
−126.0
−125.5
−125.0
−124.5
−124.0
Longitude
d
200
400
600
800
1000
1200
Isobath (m)
11/5/2017
50
100
150
C to D dist (km)

Figure 7.

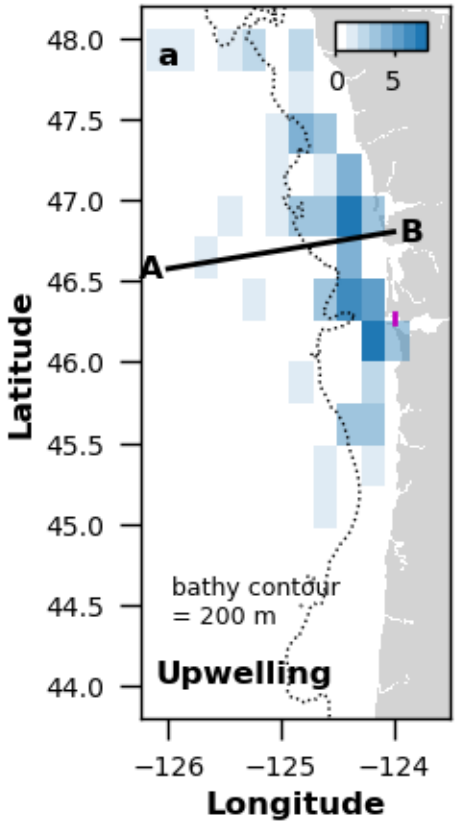
a
0
5
A
B
bathy contour
= 200 m
Upwelling
Latitude
Longitude
48.0
47.5
47.0
46.5
46.0
45.5
45.0
44.5
44.0
−126
−125
−124

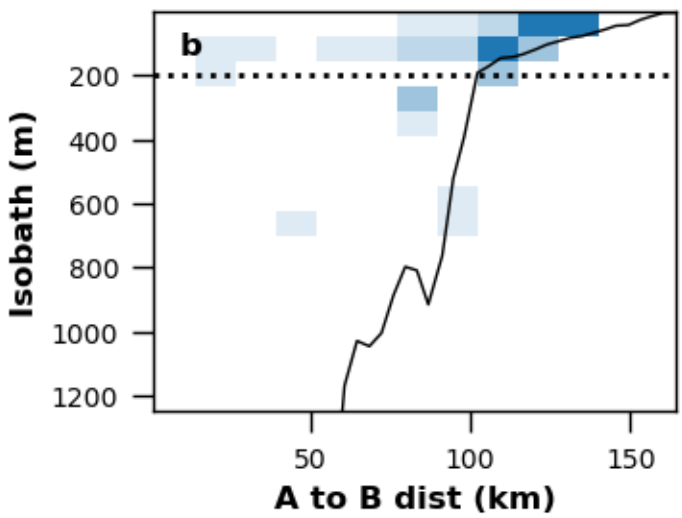
b
Isobath (m)
A to B dist (km)
200
400
600
800
1000
1200
50
100
150

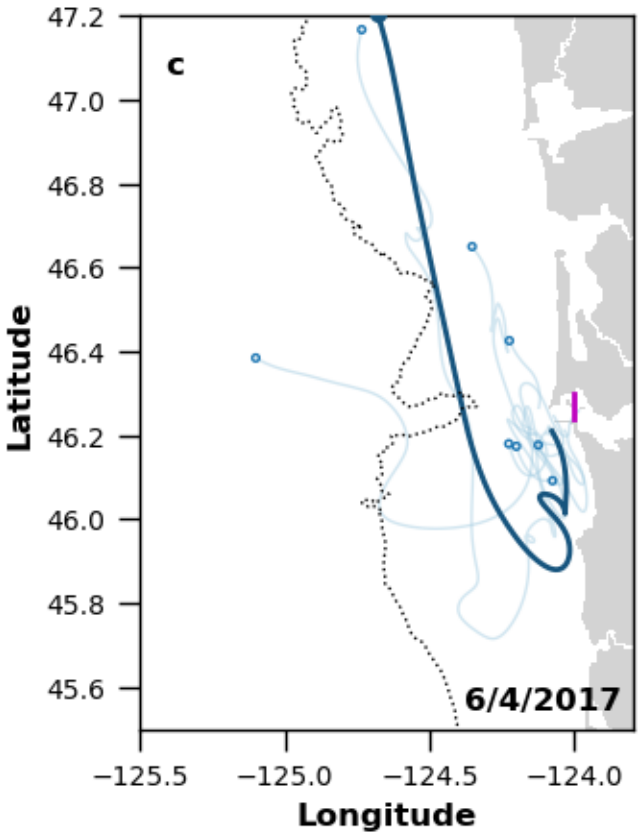
c
6/4/2017
Latitude
Longitude
47.2
47.0
46.8
46.6
46.4
46.2
46.0
45.8
45.6
−125.5
−125.0
−124.5
−124.0

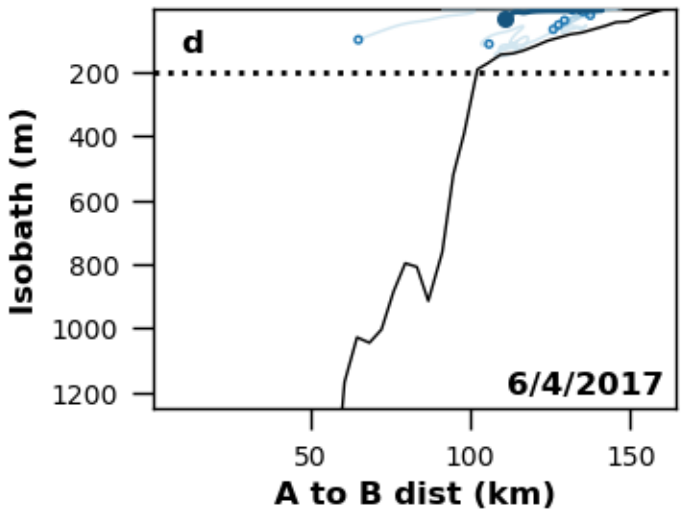
d
6/4/2017
Isobath (m)
A to B dist (km)
200
400
600
800
1000
1200
50
100
150

Figure 8.

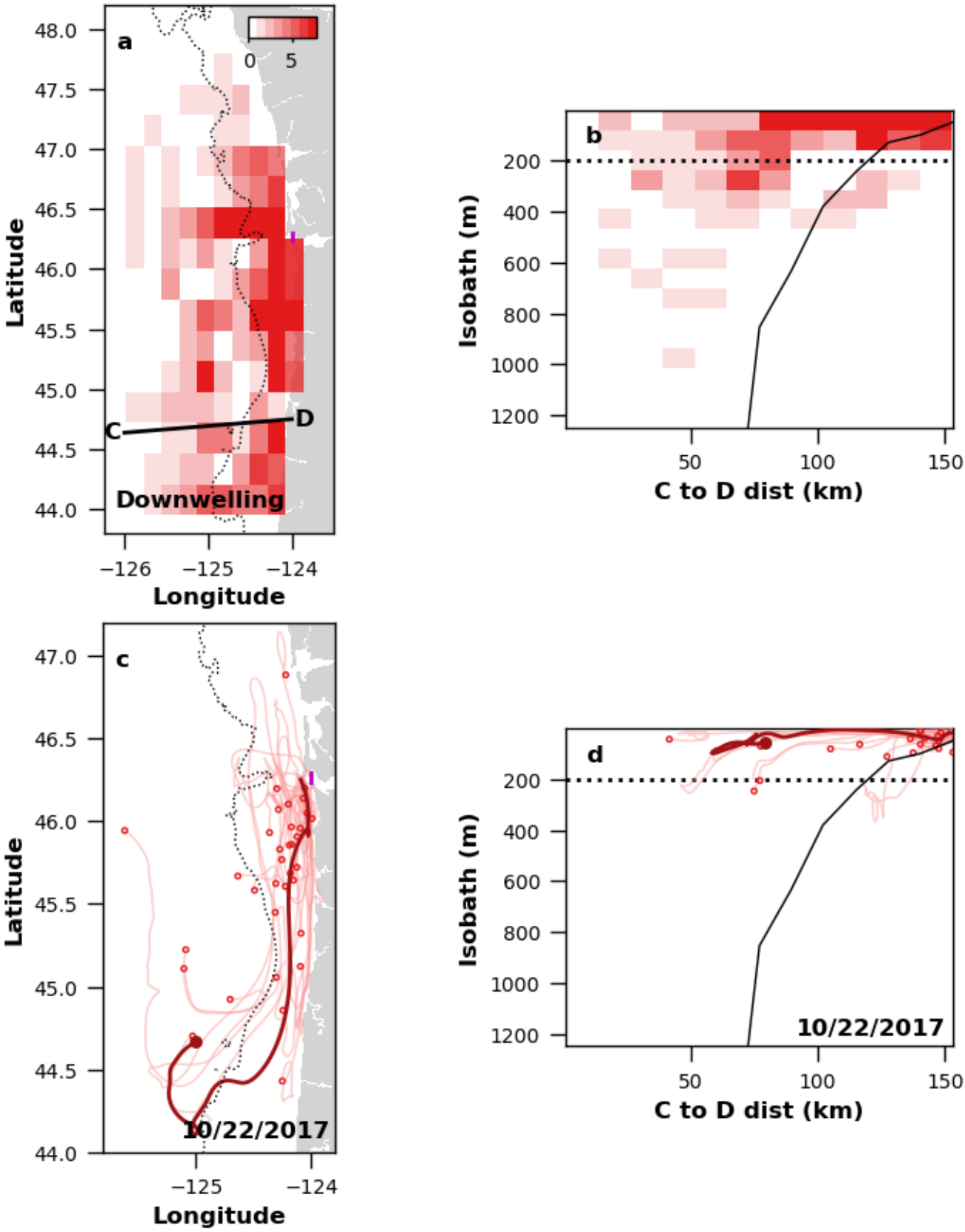
a
0
5
48.0
47.5
47.0
46.5
46.0
45.5
45.0
44.5
44.0
Latitude
C
D
Downwelling
−126
−125
−124
Longitude
b
Isobath (m)
200
400
600
800
1000
1200
50
100
150
C to D dist (km)
c
47.0
46.5
46.0
45.5
45.0
44.5
44.0
Latitude
10/22/2017
−125
−124
Longitude
d
Isobath (m)
200
400
600
800
1000
1200
10/22/2017
50
100
150
C to D dist (km)

Figure 9.

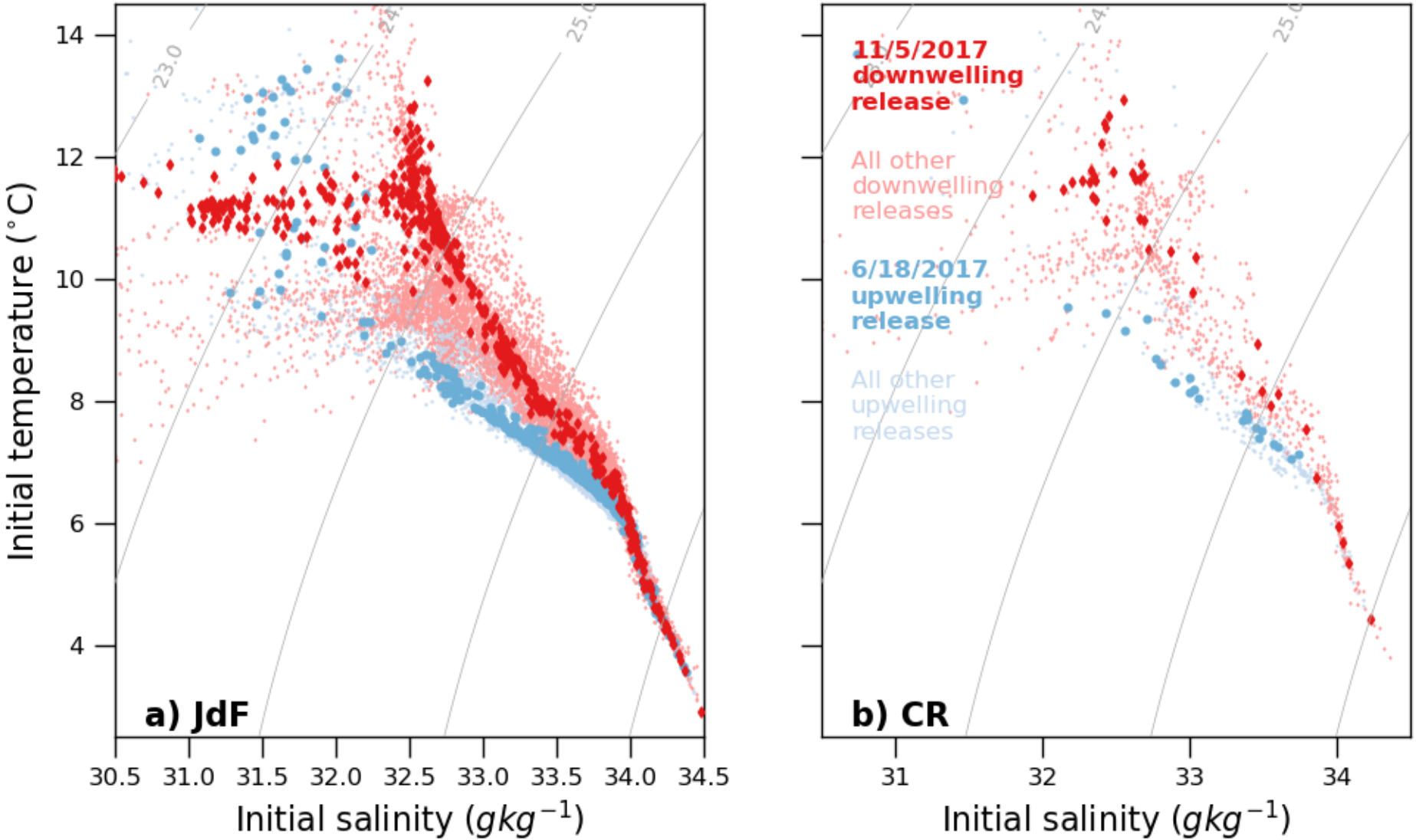
Initial temperature (°C)
14
12
10
8
6
4
23.0
24.0
25.0
a) JdF
30.5
31.0
31.5
32.0
32.5
33.0
33.5
34.0
34.5
Initial salinity (gkg^{-1})
11/5/2017
downwelling
release
All other
downwelling
releases
6/18/2017
upwelling
release
All other
upwelling
releases
b) CR
31
32
33
34
Initial salinity (gkg^{-1})